Renewable Energy 241 (2025) 122362

Contents lists available at ScienceDirect

Renewable Energy

journal homepage: www.elsevier.com/locate/renene

Multi-objective optimization of co-located wave-wind farm layouts supported by genetic algorithms and numerical models

Felipe Teixeira-Duarte [a,b,*], Paulo Rosa-Santos [a,b], Francisco Taveira-Pinto [a,b]

[a] Hydraulics, Water Resources and Environmental Division, Department of Civil Engineering, Faculty of Engineering of the University of Porto, 4200-465, Porto, Portugal
[b] Marine Energy Research Group, Interdisciplinary Centre of Marine and Environmental Research of the University of Porto - CIIMAR, 4400-465, Porto, Portugal

ARTICLE INFO

Keywords:
WEC
Layout optimization
Genetic algorithm
SNL-SWAN
Offshore renewable energy
Co-located wave-wind energy farms
K-means

ABSTRACT

This study introduces a novel methodology for optimizing Wave Energy Converter (WEC) positioning in an array using a continuous domain, surpassing the traditional fixed layout approaches. The Wave Energy Park Layout Assessment Index (WLA), which integrates the wave protection factor (HRA) and power absorption efficiency (q-factor), is employed to evaluate the performance of WEC farms. To enhance computational efficiency, unsupervised classification methods, such as k-means clustering, are used to reduce the number of sea states while accurately representing wave energy, preserving 90 % of incoming wave energy. Genetic algorithms, integrating the SNL-SWAN hydrodynamic model, are then used to optimize WEC layout by balancing exploration and computational cost, maintaining solution diversity, and avoiding premature convergence. Compared to the non-optimized designs, the proposed method increases absorbed wave power by 87 % and wave height reduction by 46 %. The study acknowledges trade-offs between objectives and area restrictions, and provides an open-source code for further research and development in WEC farm optimization. This integrated approach aims to enhance the efficiency and effectiveness of WEC farm designs, offering a robust framework for future advancements in wave energy extraction.

List of abbreviations

H_s	Significant wave height
Θm	Mean wave direction
Kt	Transmission Coefficient
LCoE	Levelized Cost of Energy
O&M	Operation and maintenance
PTO	Power take-off
T_e	Wave energy period
WEC	Wave energy converter
P_{array}	power of the entire array
q	q-factor of an array
$\sum P_{wec}$	Summation of the power output of each single isolated device in the array
SNL	Sandia National Laboratory
SWAN	Simulating Waves Nearshore model
EA	Evolutionary algorithms
GA	Genetic algorithms
WFA	WindFloat Atlantic project Turbine
GEBCO	General Bathymetric Chart of the Oceans
IHO	International Hydrographic Organization
IOC	the Intergovernmental Oceanographic Commission of UNESCO
WLA	Wave Energy Park Layout Assessment Index
HRA	Reduction in significant wave height within the protected area index
AOI	Area of interest
MAPE	Mean Absolute Percentage Error
RMSE	Root Mean Square Error
GMM	Gaussian mixture models
VBGMM	Variational Bayesian Gaussian mixture models
φ_p	power representativeness

1. Introduction

In the transition towards a more sustainable energy system, wave energy has significant potential due to its abundant, predictable, and high-density resource [1]. However, the high Levelized Cost of Energy (LCoE) caused mainly by immature technologies hinders its progress. Understanding wave farm effects (diffraction, reflection, radiation) on energy capture and their dependence on WECs' layout is crucial for their optimized design [2], which aims to maximize energy output, eventually explore co-location benefits (*e.g.*, with offshore wind farms), and

* Corresponding author. Departamento de Engenharia Civil, Faculdade de Engenharia da Universidade do Porto, Rua Dr. Roberto Frias, s/n, 4200-465, Porto, Portugal.
E-mail address: up200908769@edu.fe.up.pt (F. Teixeira-Duarte).

https://doi.org/10.1016/j.renene.2025.122362
Received 12 July 2024; Received in revised form 23 December 2024; Accepted 7 January 2025
Available online 9 January 2025

minimize costs and environmental impacts.

Portugal's focus on offshore wind (10 GW targeted by 2030 [3]) creates an opportunity for co-location with wave energy [4,5]. This option offers synergies that may range from dual energy conversion and lower overall costs to improved accessibility for offshore wind farm maintenance [6–13] since wave parks can act as wave attenuators, creating a "shadowing" effect that protects the wind turbines [14,15]. This is particularly relevant as offshore wind farms are burdened by significant operation and maintenance (O&M) costs, reaching 30%–35 % of their lifetime expenses [4]. Therefore, the industry is shifting towards preventive and predictive maintenance strategies to reduce these costs [5]. The high construction and O&M costs are also a major barrier for wave energy farms [16]. Fortunately, combining offshore wind turbines with WECs creates an opportunity to share infrastructure, electrical systems, and operational resources, thereby reducing overall costs [17].

The increased energy yield is also among the primary motivations for exploring combined wind and wave energy arrays [18], with wave energy offering greater predictability compared to wind energy [6]. Additionally, their lagging can benefit battery storage systems and potentially reduce the required combined power capacity, leading to a smoother and more continuous power output. The integration of wave energy can also reduce intermittency-related balancing costs in the power grid [3].

Expanding on these co-location benefits, offshore wave farms can also serve a secondary purpose – coastal protection through wave attenuation and "*shadowing*" of sensitive shorelines [19,20], leading to lower mean wave heights [17]. However, traditional farm modeling approaches often oversimplify key aspects. These simplifications include assuming invariant transmission coefficients, fixed power ratings, and limited farm configurations. Additionally, they may neglect local marine space restrictions or utilize a small number of WEC units.

Optimizing the layout of wave farms is complex due to the numerous variables involved (WEC position, array shape), constraints (space available, already allocated areas), and conflicting objectives (energy output vs. costs vs. environment). Current design methods often neglect these aspects, focusing solely on maximizing the energy output [2]. Additionally, computational demands increase significantly with multi-objective functions or high-fidelity wave-WEC interaction models.

With limited field data available, WEC development usually relies on physical and numerical modeling. Numerical modeling, particularly through wave propagation models, is well-suited for assessing multivariable combinations. These tools can be adapted to forecast local wave climates, wave farm energy outputs, and both near-field and far-field effects [21,22].

Phase-averaged models provide a computationally efficient approach for the simulation of waves and nearshore wave-induced current fields. However, most of them rely on parametrizations to represent WECs and other relevant wave characteristics. A common technique involves representing WECs as porous structures acting as sources or sinks for wave energy extraction [23,24]. The SWAN (Simulating WAves Nearshore) spectral wave model is widely used and validated for coastal wave transformation modeling. A modified version, SWAN-SNL [25–28], allows for WEC representation as power sinks using device-specific power performance data.

The use of evolutionary algorithms (EAs), specifically genetic algorithms (GAs), provides an efficient solution to this optimization problem. EAs, inspired by natural selection, offer flexible and robust optimization frameworks, with GAs operating on candidate solutions to mimic the survival of the fittest, optimal layout, considering factors like energy output, environmental impact, and economic viability. This paper addresses the challenge of wave farm layout optimization by proposing a novel, multi-objective framework. The framework integrates three key components:

(i) Representative sea-state selection: a statistical analysis coupled with machine learning techniques is used to identify a representative set of sea states that accurately capture the local wave climate.
(ii) Multi-objective genetic algorithm optimization: a tailored GA is developed to optimize wave farm layouts for multiple objectives. This includes energy production estimated using SNL-SWAN model, alongside environmental impact considerations seamlessly integrated into the fitness function. Domain-specific operators are implemented in the GA to ensure physically feasible solutions based on established knowledge of wave-WEC interaction.
(iii) Open-source framework for reproducibility: the complete codebase is provided to facilitate replication by other researchers. This fosters further research on WEC farm optimization and coastal morphodynamic evolution.

Previous studies in WEC array optimization have extensively used fixed or small arrays in a much greater area [2,29], where the optimizations merely find the best separation distance between WECs [30–32], focused on discrete positioning strategies. For instance, many works employ grid-based methods, limiting WEC placements to predefined locations [32–42]. While these methods simplify computational demands, they inherently restrict the flexibility needed to achieve optimal layouts in realistic scenarios [43,44]. Moreover, the majority of existing studies emphasize single-objective optimization, such as maximizing power output [2,31] or focus on specific environmental conditions [17, 45,46], limiting their generalizability.

As the computational demands of evaluating WEC arrays grow exponentially with the number of converters, developing a fast and effective optimization approach for large-scale wave farms becomes crucial [47]. To address this challenge, the proposed multi-objective evolutionary algorithm optimizes both power output and hydrodynamic interactions within large-scale farms. The methodology combines a smart initialization process, a population-based evolutionary algorithm, a third-generation wave numerical model, and continuous global optimization. This integrated approach effectively handles the complexities of large-scale wave farm optimization, scaling up the array size without sacrificing computational efficiency, while accurately capturing significant interactions between WECs and managing the extensive search space dimensions inherent to the problem.

This approach departs from prior studies that often focus on single or limited objectives. It offers a more realistic solution by simultaneously considering a large number of WECs on a continuous deployment domain, variable installed capacity, and a robust statistical representation of local wave conditions. The versatile SNL-SWAN model [26,27, 48], effectively captures complex interactions and provides greater adaptability to site-specific constraints and stakeholder priorities. The proposed GA framework demonstrates its effectiveness through rigorous simulations and case studies. These studies evaluate convergence speed, solution quality, and overall robustness against existing methods. The framework excels in balancing energy extraction with environmental considerations.

The research discusses future directions, including applicability to diverse wave farm configurations, integration with advanced computational models for accuracy, and the development of self-adaptive frameworks for dynamic optimization under varying wave conditions. Overall, the work highlights the power of GA as a tool for optimizing wave farm layouts. By facilitating efficient wave energy harvesting while considering environmental and economic constraints, GA-based optimization holds significant promise for unlocking the potential of wave energy and contributing to a sustainable future powered by ocean renewables.

The paper is organized as follows: Section 2 presents the methodological framework, detailing the chosen case study region, evaluation parameters, WEC technology, numerical model, and the multi-objective

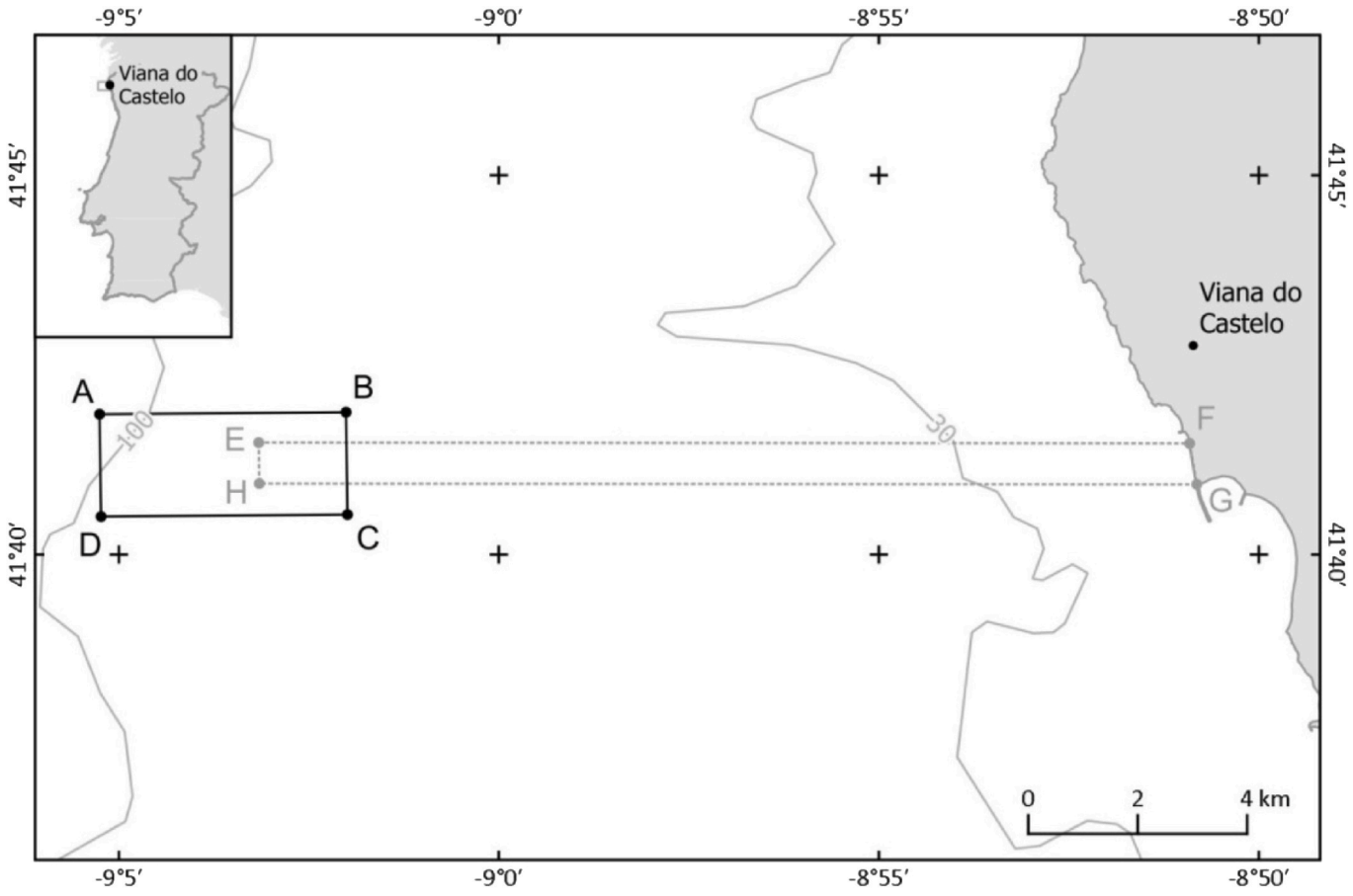

Fig. 1. Location of the WindFloat Atlantic farm. ABCD are the vertices of the protection area and FEGH the submarine cable area [50].

Table 1
Coordinates (WGS84) of the protection area vertices and the wind turbines [51].

Vertex	Latitude (°)	Longitude (°)
A	−9.0875989	41.697497
B	−9.0335472	41.697934
C	−9.0332331	41.675428
D	−9.0872658	41.674992
WFA3	−9.0501671	41.686668
WFA1	−9.0574999	41.686501
WFA2	−9.0646667	41.686501

GA formulation. Section 3 delves into the statistical analysis employed for sea-state selection. It elaborates on the implementation of the unsupervised classification model, along with considerations regarding model accuracy, validation, and convergence. Section 4 showcases the key findings of the wave farm layout optimization process. This section discusses the proposed solutions, drawing support from metrics associated with energy output, environmental impact (shielding protection), and computational efficiency. Finally, Section 5 summarizes the study's primary contributions, offering practical considerations and recommendations for future research.

2. Methodology

2.1. Case study site

The case-study site is located offshore Viana do Castelo (Northern Portugal), where the offshore farm of WindFloat Atlantic project is located. This wind farm is composed of three floating wind turbines with a total installed capacity of 25 MW, and is located between 17 and 19 km from the coast of Viana do Castelo, where water depths can reach 100 m [49]. The wind farm positioning area is 4.77 km^2, and the protection area is 11.25 km^2 [50]. Fig. 1 presents the location of WindFloat park and Table 1 the vertices' coordinates of the protection area and the wind turbines (WFA) [51].

The bathymetry data used were obtained from the datasets of GEBCO (The General Bathymetric Chart of the Oceans), which operates under the joint support of the International Hydrographic Organization (IHO) and the Intergovernmental Oceanographic Commission (IOC) of UNESCO.

2.2. Parameters and deployment area

This research work builds upon previous work [14], which introduced a new multi-objective index for evaluating WEC farm layouts: the Wave Energy Park Layout Assessment Index (WLA). This index combines two separate metrics: the reduction in significant wave height within the protected area (HRA) and a factor representing the power capture efficiency (q-factor).

Unlike previous work [14], which employed fixed layouts for the WECs, this study utilizes a continuous domain for WEC placement. This approach allows for greater flexibility, as WEC locations can be freely optimized within the designated area, adhering only to minimum distance constraint between WECs. To initiate the optimization process, the initial layout was generated by randomly placing WECs within the allowable domain. Fig. 2 depicts one such initial layout alongside the selected placement area.

The HRA evaluates the reduction in significant wave height (H_s) within the designated area of interest (AOI) protected by the WEC farm. The AOI is defined as the rectangular area around the turbines, ensuring a minimum distance from each turbine (*e.g.*, 1600 × 400 m with a 200 m

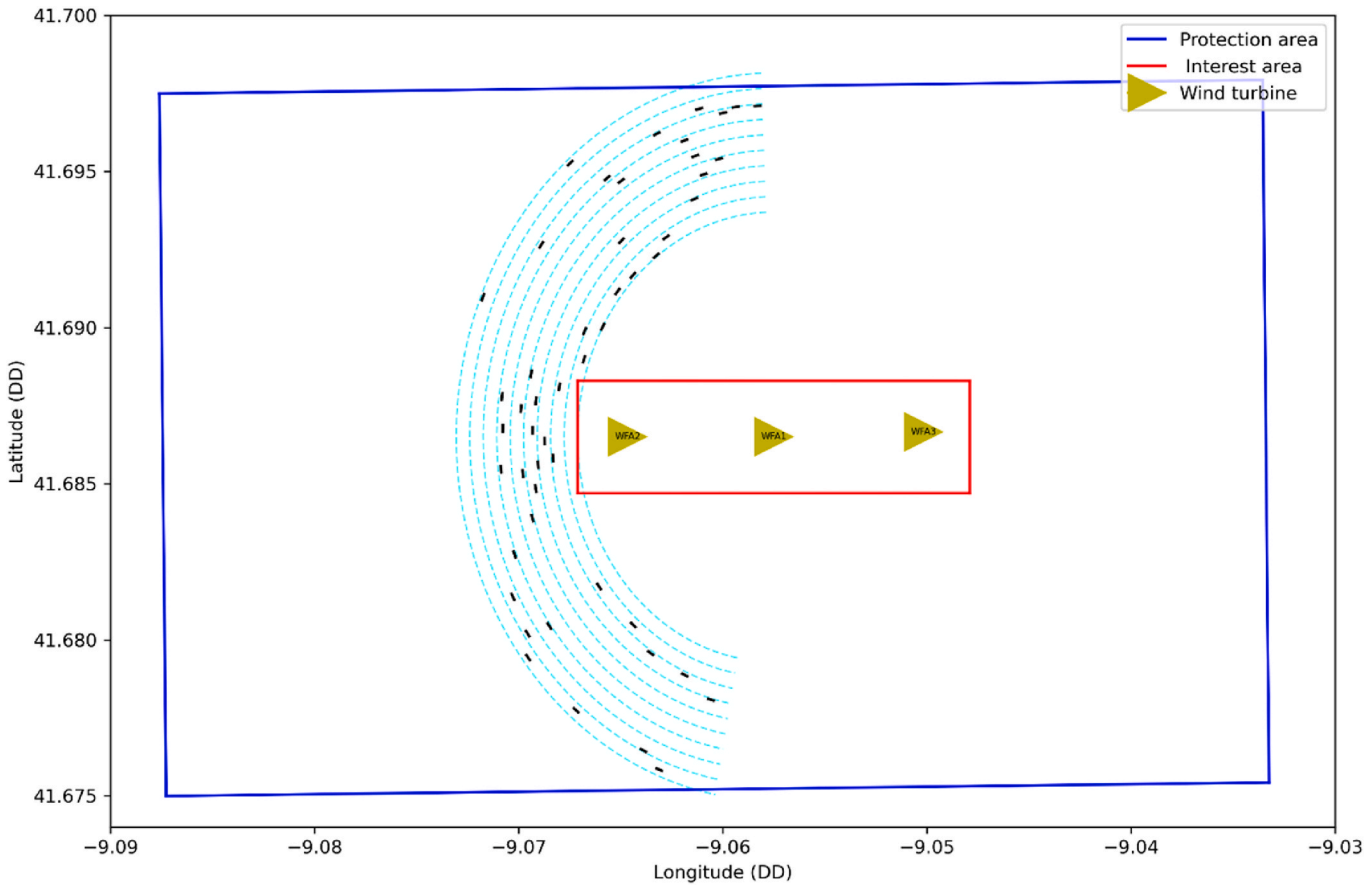

Fig. 2. Protection area (dark blue), WEC farm possible area (light blue), area of interest (red), and wind turbines (yellow). (For interpretation of the references to color in this figure legend, the reader is referred to the Web version of this article.)

buffer as depicted in Fig. 2). The HRA index is calculated using:

$$HRA = \frac{100}{n} \sum_{i}^{n} \frac{Hs_i - Hs_{wec_i}}{Hs_i} \quad (1)$$

where i represents a calculation node within the AOI, n is the total number of nodes, Hs_i is the significant wave height on the i^{th} node in the baseline scenario (without the WEC farm), and Hs_{wec_i} is the significant wave height on the i^{th} node with the WEC farm.

A common metric used to assess WEC farm performance is the q-factor, since it provides a simple way to quantify how WEC interactions affect overall power absorption. The q-factor is defined as the ratio between the power absorbed by the entire array, P_{array}, and the summation of the power that can be absorbed by each single WEC in the array individually (*i.e.* without the influence of the other WECs), P_{wec}, *i.e.*,

$$q = \frac{P_{array}}{\sum P_{wec}} \quad (2)$$

To aid decision-making and selecting the optimal WEC farm layout based on stakeholder priorities, the Wave Energy Park Layout Assessment Index (WLA) was developed. This index combines two seemingly opposing metrics – the HRA (wave protection) and the q-factor (wave power absorption) - to provide a comprehensive performance evaluation.

The WLA index normalizes HRA and q-factor values and produces an output ranging from zero to one, with one representing the most favorable choice among the alternatives,

$$WLA = pN(q) + sN(HRA) \quad (3)$$

where p ($p = 1 - s$) is the weighting factor for the power absorption, and s is the weighting factor for the wave protection (shielding). The WLA index employs a min-max normalization (N), *i.e.*, a rescaling technique, to put HRA and q-factor values into a range between 0 and 1. This normalization ensures a consistent and comparable scale for both metrics within the final WLA index.

By incorporating weighting factors for power absorption and wave protection, the WLA index allows stakeholders to prioritize their desired outcome, hence resulting in a more informed decision-making process for WEC farm layout design.

To have more insights on the array efficiency relative to the number of devices it was also analyzed the Capture Width Ratio (CWR), which is a widely used metric for evaluating the hydrodynamic efficiency of a WEC. It represents the proportion of wave energy absorbed by the device relative to the energy flux available within its characteristic length. This efficiency is expressed as a ratio of the power absorbed by the WEC to the product of the wave energy flux per unit width and the characteristic length of the device.

The characteristic length, L, is often defined as the physical width of the WEC that is perpendicular to the wave front. In this study, L corresponds to the overall width of the CECO. The CWR can be expressed as:

$$CWR = \frac{P_{abs}}{J.L}$$

where P_{abs} is the power captured by the WEC, J is the wave energy flux per meter of wave front, and L is the device's characteristic width. Unlike absolute measures of absorbed energy, the CWR offers a dimensionless perspective on the performance of a device. By normalizing energy capture relative to the device's size, it becomes easier to compare different WECs, regardless of their physical dimensions or operational scales. This makes the CWR particularly useful for benchmarking and

Table 2
Principal features of CECO (Key parameters for this investigation are in bold).

Parameter	Value
PTO inclination angle (°)	30
LMM inclination (°)	45
LMM length (m)	9.52
LMM width (m)	6
LMM maximum stroke (m)	15
LMM mass (ton)	288
Overall width (m)	**22**
PTO rated power (kW)	**500**

performance optimization.

2.3. Wave energy converter

In this study, the floating version of CECO [52–54] device was used as a case study for capturing wave energy. CECO is a point absorber WEC that utilizes a sloped power take–off (PTO) system [53], allowing it to capture both the vertical and horizontal force components of ocean waves [55,56]. The main elements of the CECO consist of two lateral mobile modules (LMMs) connected by a frame of tubular elements. In its current design, CECO uses a rack and pinion system to convert the absorbed energy into electricity [52].

The CECO's design is still under development and continues to evolve as research progresses. Table 2 summarize the principal features of CECO. Since, there has not been much studies done on the impacts of CECO farms, this study uses the results of Ramos et al. [57], obtained for the same site, as a starting point. The authors proposed an arrangement of CECO units placed on a curvilinear alignment facing the prevailing wave direction (NW or 315°).

The SNL–SWAN model uses the WEC power matrix to establish the frequency dependent transmission coefficients. Fig. 3 presents the power matrix of CECO [57] used as an input in the model.

2.4. SNL-SWAN

The model SNL–SWAN [25,58] refers to the improvements that Sandia National Laboratories made in SWAN to allow a more accurate evaluation of WEC farm effects on wave propagation, considering also the dependence of WEC performance on it. The model's accuracy has been verified and preliminarily validated against data from controlled wave tank experiments [26–28]. SNL–SWAN includes new types of obstacles that allow calculating transmission coefficients (kt) based on the WEC power performance obtained from its power matrix or its relative capture width curve. The model also permits frequency–dependent wave energy transmission through obstacles. In fact, this method enables the transmission coefficient (linked to wave power absorption) to vary when wave conditions change over a relatively broad range of temporal and spatial scales.

Furthermore, SNL-SWAN incorporates more comprehensive physical processes, allowing for a more accurate representation of wave behavior within WEC arrays. Additionally, the model grants greater control over simulation parameters, which enables to input more precise data and fine-tune settings to achieve a more realistic simulation environment. SNL-SWAN also has greater flexibility compared to the original SWAN. In essence, SNL-SWAN emerges as a powerful tool, significantly improving upon SWAN's capabilities for simulating ocean waves and evaluating WEC performance.

Preliminary studies with the SNL–SWAN model have already been conducted for the case study site – the WindFloat Atlantic wind farm

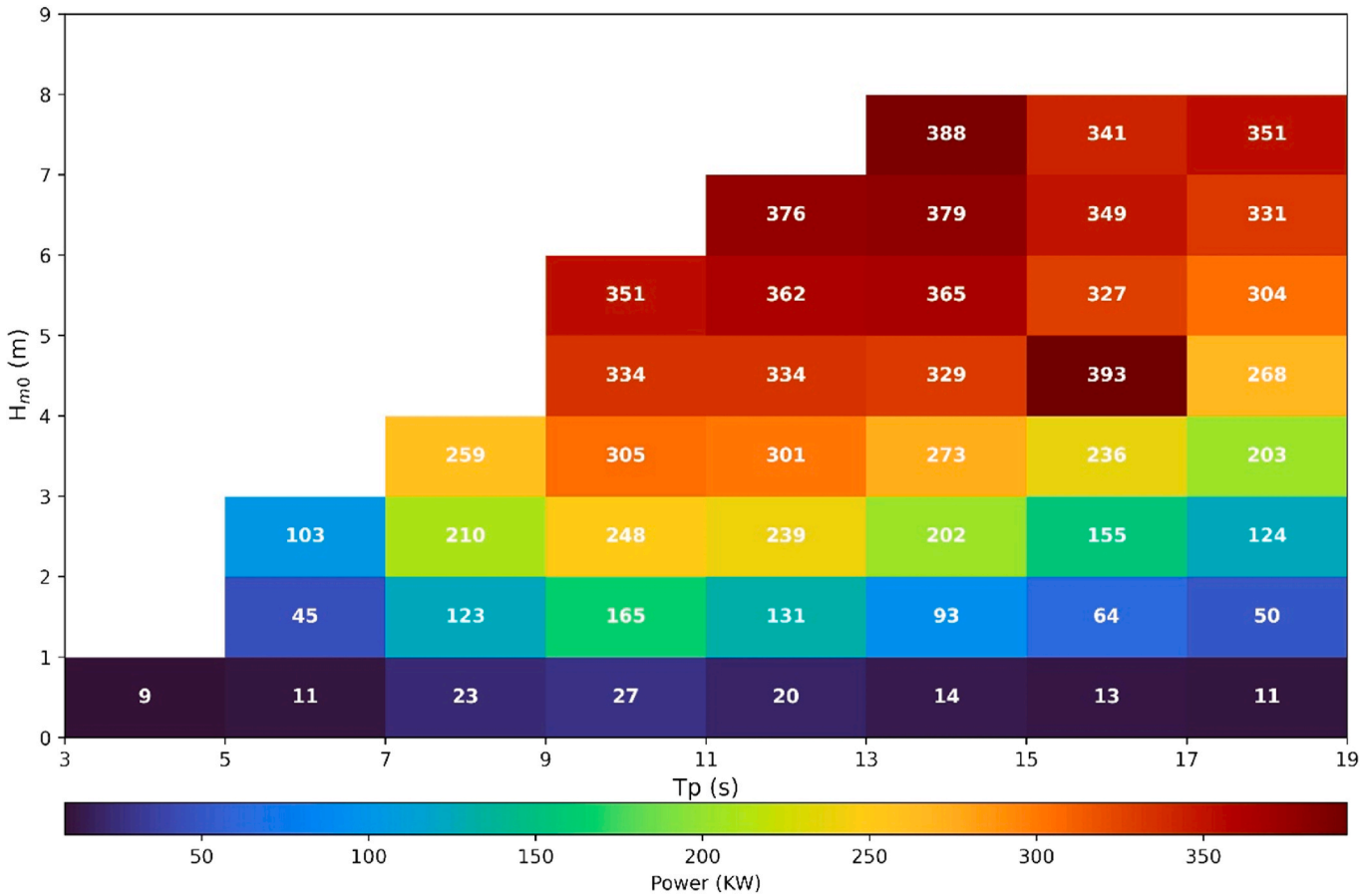

Fig. 3. Power matrix for CECO. It shows the average power output for each sea state conditions (adapted from Ref. [57]).

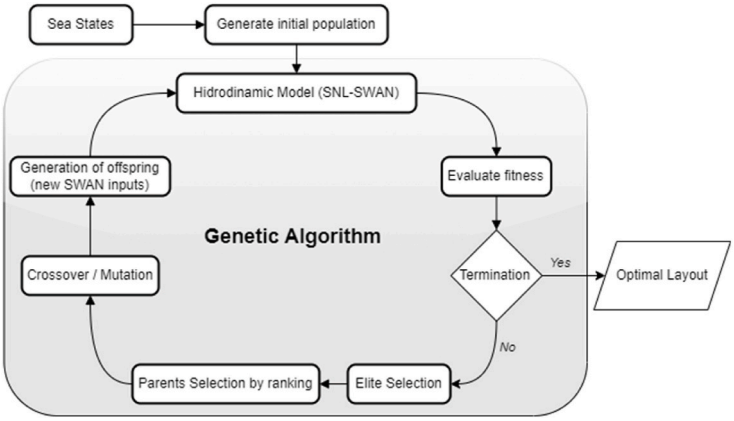

Fig. 4. Genetic Algorithm loop.

located offshore Viana do Castelo in the Northern coast of Portugal – focusing on co–located offshore energy farms and on analyzing their impact on wave climate. The objective was to investigate the potential effects of an array of WECs on leeward wave propagation and its synergies with the already installed wind farm [59]. Furthermore, the study aimed to establish the multi–objective function to examine and choose between WECs arrays.

This study uses a frequency-dependent transmission coefficient based on the WEC's power absorption matrix at each wave frequency. While this approach offers advantages, it has some limitations. SNL-SWAN does not account for diffracted or radiated waves generated by WEC operation. Additionally, resonance phenomena and the potential formation of standing waves within the WEC array are not captured. These factors can influence WEC power absorption, and their omission contributes to a shared limitation between SNL-SWAN and the standard SWAN model [30].

Despite these limitations, SNL-SWAN remains the preferred choice for assessing environmental and far-field impacts of WEC farms compared to alternative models like RANS/SPH-CFD, coupled BEM and Boussinesq, mild-slope, and non-hydrostatic models [30]. This preference stems from SNL-SWAN's key strength: ability to simulate wave propagation across extensive coastal areas with varying bathymetry at an acceptable/manageable computationally cost. In contrast, potential flow models, while offering higher accuracy in some aspects, lack the flexibility to handle complex bathymetric features and are more demanding computationally.

2.5. Unsupervised classification for minimal representative sea states

The efficiency of the GA model in WEC farm optimization is highly dependent on the number of sea states considered. Since GA simulations require evaluating each population member (layout) under all sea states across generations, the computational cost increases significantly with additional sea states. For instance, in a scenario with 50 individuals, a 95 % crossover rate, and 100 generations, adding just one sea state would result in over a 4000-fold increase in simulations (Scenario S4, see Table 6). This exponential growth can become a major bottleneck, especially considering the vast amount of data (nearly 600,000 entries). Nevertheless, the unsupervised learning techniques effectively deal with massive volumes of data [60].

Unsupervised classification is a fundamental method in machine learning and data mining, allowing for the automatic discovery of hidden patterns and structures within unlabeled datasets, attributes or characteristics. The process involves representing the data, defining a distance or similarity measure, initializing the clusters, assigning data points to the clusters, iteratively refining those clusters, and evaluating the results. The group assignment is done based on the similarity to cluster centroids. The quality of the clusters can be evaluated using both internal or external metrics. Different clustering algorithms exist, each employing different strategies and assumptions based on the nature of the data and the problem at hand.

Some studies applied clustering methods to wave climate estimation, mostly k–means, to deal with the huge amount of data [60–68]. The k–means clustering algorithm can be applied to metocean data (e.g., significant wave heights, H_S, peak wave periods, T_P, peak wave directions, θ m) to analyze and understand local extreme events, as well as to characterize waves and currents. In this context, k–means clustering aims to identify distinct groups or clusters within the dataset based on the values of H_S, T_P, and θ m [66], to reduce the number of sea states needed for the study.

The unsupervised classification methods utilized included k-means, Gaussian Mixture models (GMM), and Variational Bayesian Gaussian Mixture models (VBGMM). These methods were implemented using the python scikit-learn library [69] with the full and filtered dataset. The approach followed the normalization procedure outlined by Camus [60], to equalize the scales.

To assess the effectiveness of sea state clustering, this study employed two common error metrics: Mean Absolute Percentage Error (MAPE) and Root Mean Squared Error (RMSE) [28]. These metrics are widely used to evaluate model predictions providing valuable insights on the representativeness of each cluster regarding the corresponding sea states [70]. Notably, previous research [62–65] used metrics similar to MAPE to evaluate input wave parameters within k-means clustering applications.

2.6. Genetic algorithm optimization

The genetic algorithms (GA) are the most recognized type of evolutionary algorithm and have been applied several times as optimization function and search method [71]. These are robust methods that do not necessitate derivative information and can manage a huge number of variables to determine the minimum or the maximum of a function. Usually, these algorithms have a binary representation, a low probability of mutation, and an emphasis on genetically inspired recombination to determine the selection of fittest, to generate the new candidate solutions.

The algorithm flow is inspired by the continuous Darwinian improvement cycle of evaluation [72]. In GA, the survivability, or fitness, is evaluated by a selection operator, which determines the solutions that best solve the problem with minimum error. The individuals of the populations are evaluated according to the objective function, the fitness. An evaluation step is a non–deterministic approach. The repetition of the process for several generations, the probability disseminates genes that promote higher fitness, creating better solutions and extinguishing the worse suited [31].

This study used an initial population of 500 random individuals

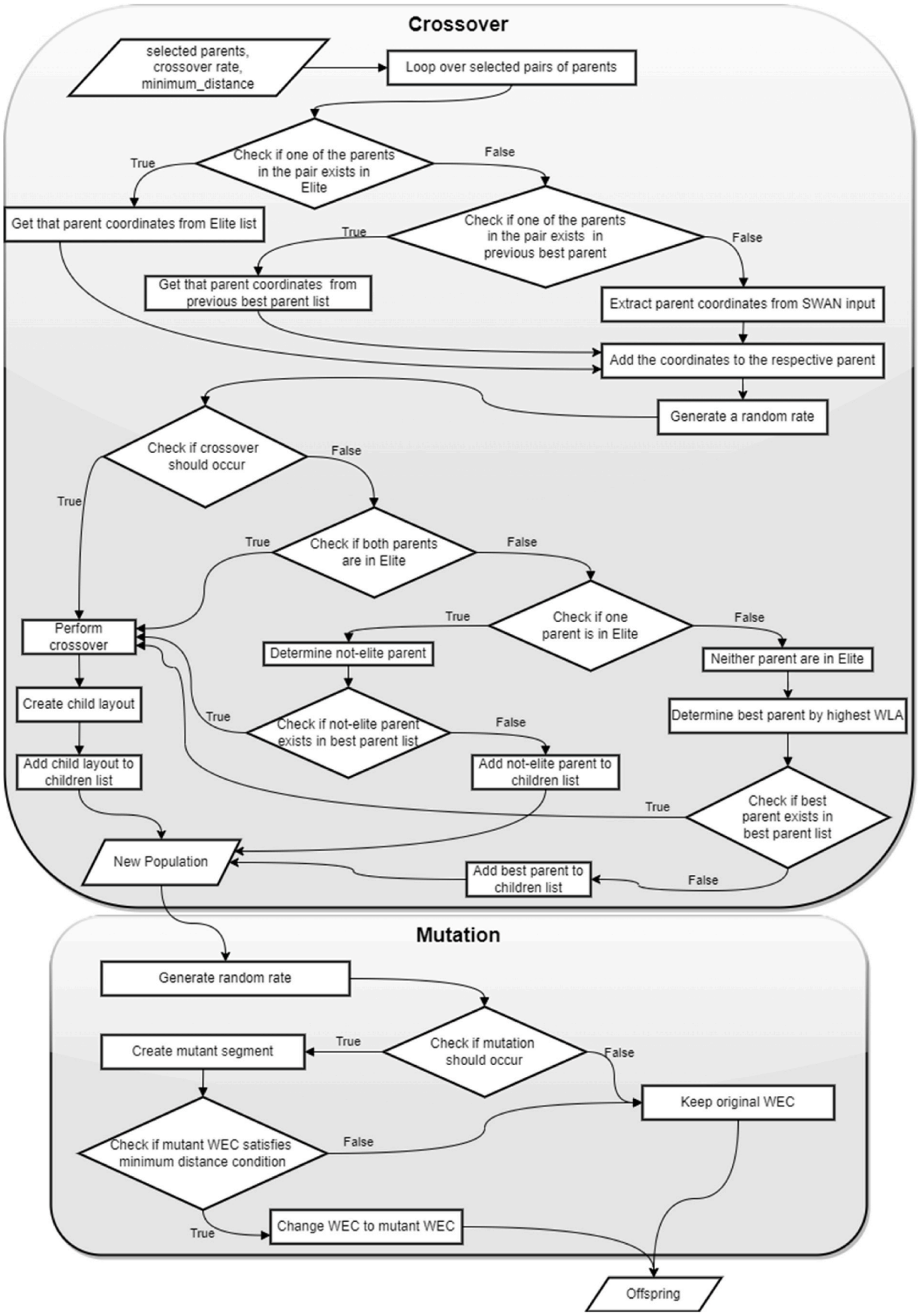

Fig. 5. Flowcharts of crossover and mutation functions inside the genetic algorithm.

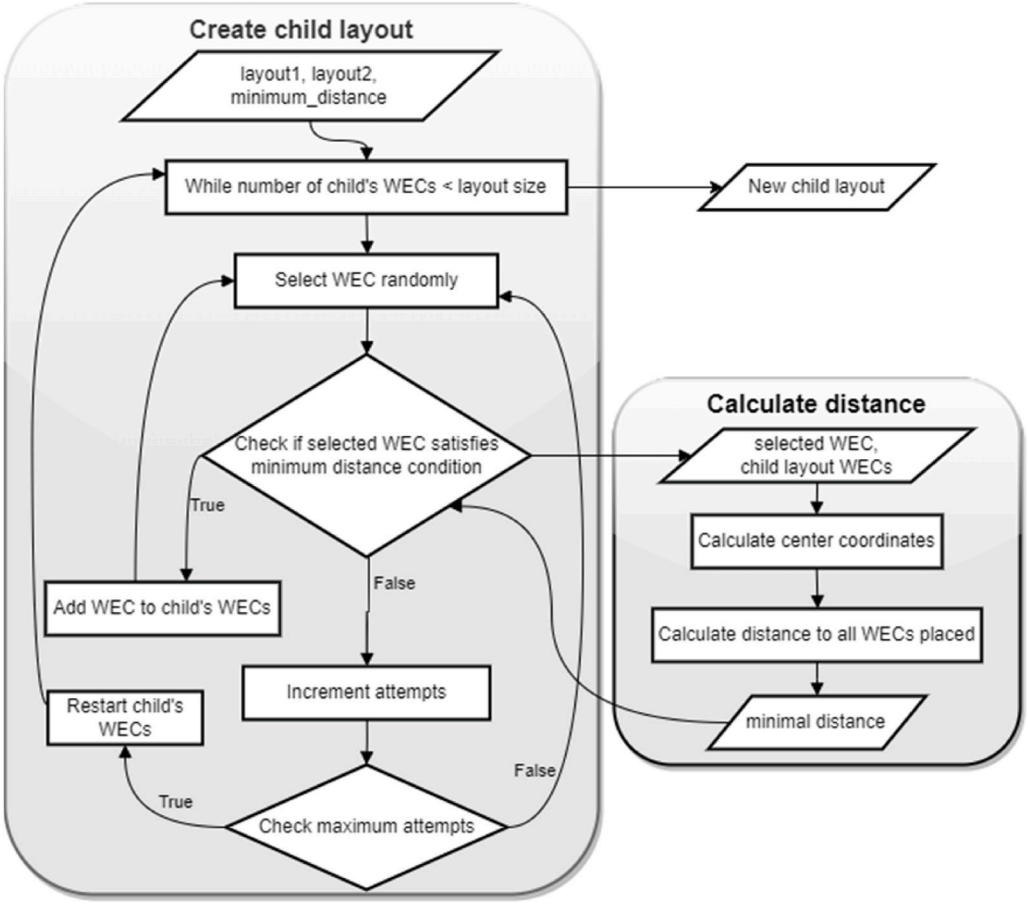

Fig. 6. Flowcharts of the function to create new (child) layout simulating reproduction between two previous generation layouts (parents).

Table 3
Statistical description of wave data parameters.

	Hs (m)	Tp (s)	Θm (°)
Mean	1.9	10.2	295
Standard Deviation	1.2	2.4	30
Minimum	0.1	2.4	0
Quantile 25 %	1.1	8.5	281
Quantile 50 %	1.6	10.1	299
Quantile 75 %	2.5	11.8	315
Maximum	10.4	23.6	359

(WEC farm layouts). Then the workflow of GA enters in a loop, Fig. 4 [12]. The SNL-SWAN model is incorporated inside the GA loop. At the beginning, the model simulates all initial population for every sea state, generating 2 outputs: the power absorption of each WEC and the H_S of every node in the AOI. Those outputs are processed in the evaluation code, and generate a table with weighted mean H_S reduction and power absorption for each layout.

The fitness evaluation uses the WLA index [14] to classify the layouts and determine the elite that will be granted in the next generation. The parents' selection is done using the probability according to the individual ranking, *i.e.*, individuals of higher rank have higher changes to be picked, independently of their WLA value. It is worth noting that even with a low probability of choosing the same pair of parents more than once, the creation of new individuals is forced to be different from the ones already in the offspring.

The reproduction was performed applying the crossover and mutation, according to the flowchart in Fig. 5, using the function "*create child layout*" described in the flowchart presented in Fig. 6, which combines the WECs from the parents regarding the minimal distance between WECs constrain.

The crossover flowchart outlines the selection process for elite individuals and best parents, which are individuals preserved even when the crossover operation is bypassed due to the crossover rate, used to populate the next generation. This ensures the retention of valuable genetic information from the previous generation. The information for all individuals, including offspring generated by crossover and elite members from the prior generation, is retrieved from a dictionary data structure. Then, the crossover loop iterates through each crossover rate, determining whether crossover should be applied based on the pre-defined probability.

To maintain population diversity and prevent duplicates, a check for repeated individuals is done after the crossover operation. This ensures that the newly formed population adheres to the principle of a unique solution space within the GA. Finally, the complete population undergoes mutation, introducing random variations within each WEC (segment) while adhering to the pre-defined layout constraints. This mutation process injects novelty into the population, facilitating the exploration of the solution space.

Generating offspring layouts (children) within a continuous domain presents a challenge due to the minimum distance constraint between individual WECs. This function, illustrated in Fig. 6, addresses this challenge by randomly selecting a WEC from either parent layout. The selected WEC's position is then evaluated to ensure it adheres to the minimum distance requirement from previously placed WECs in the

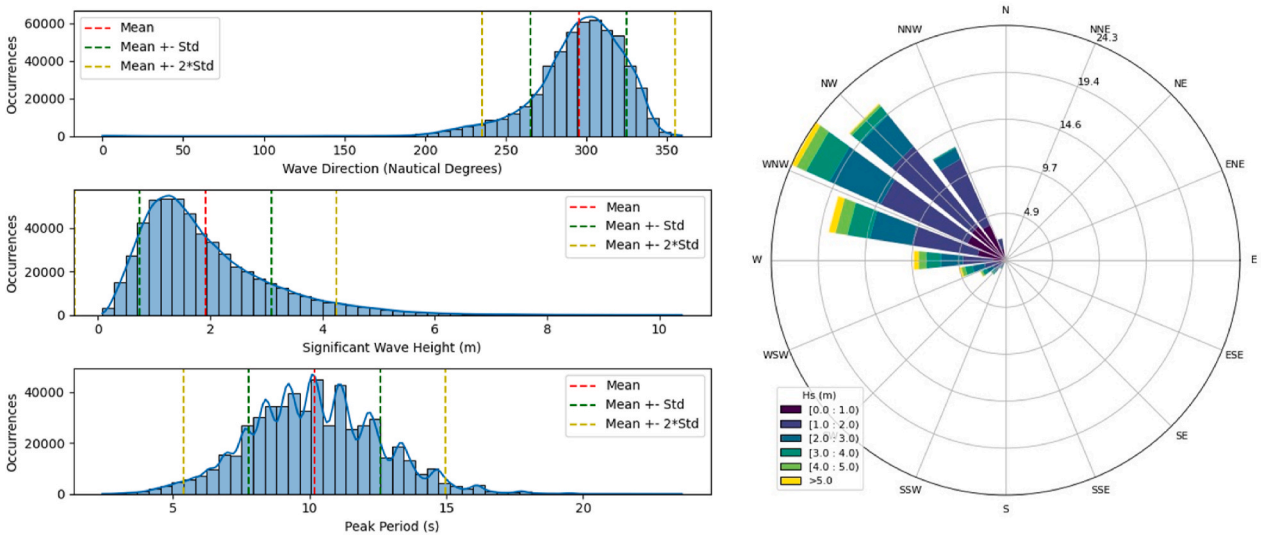

Fig. 7. Normal distribution of the wave parameters and a wave rose of the location.

child layout.

However, this approach can potentially lead to deadlocks where the remaining WECs cannot be positioned within the constraints. To mitigate this, a limit is set on the number of placements attempts for each WEC. If this limit is reached without a successful placement, the reproduction process restarts. This mechanism ensures that even if the parents are highly similar, a valid child layout satisfying the minimum distance restriction will eventually be generated.

There are two possible ways that an individual from previous generations survive to the next one. The first one is that it belongs to the elite of that generation, which assures that the best individuals of the generation are not lost in the reproduction process. The second one is when the crossover does not occur, *i.e.*, the rate of occurrence of that matting is lower than the crossover rate predefined. In this case, the best parents are repeated in the next generation after a chain of checks to ensure no individual repetition in the offspring.

While the value of each fitness is important to determine the chances of individual survival, there is no guarantee that the ones with the higher fitness values will survive or the ones with the smaller values will perish, because of the non–deterministic nature of the method [73]. Given that, it could occur that some individuals with low fitness value genes might prove to be useful when recombined in new chromosomes, which is a low probability "second chance", offered by the process flexibility that would be impossible in a more deterministic setting [73].

2.7. Optimization problem definition

In this study, the optimization problem is designed to maximize the WLA index in each generation, as presented in Ref. [14] and summarized in Section 2.2. *Therefore, globally, it will maximize a combination of the q-factor and the HRA according to specified weights that reflect the importance given to each factor. For demonstration purposes, in this study equal weights (p=s) were assigned to ensure a balanced contribution from both factors.*

The algorithm adjusts the positions of the WECs to find the optimal layout. The position of the WECs is constrained by sector bounds, where WECs are limited to a deployment sector between directions 213° and 338°, as defined in Section 3 based on the predominant wave energy direction, and by a radial distance. Where WECs are be placed at a distance from the AOI boundary to 10 times the minimal distance between WECs. This deployment area was defined according to the protection area of the WindFloat Atlantic farm [57].

The selection of the crossover rate and population size was driven by their influence on the required number of SWAN simulations for each layout. Given the computationally intensive nature of multiple SWAN simulations, it was imperative to carefully consider these parameters to strike a balance between solution quality and computational cost. To optimize the trade-off between exploration and exploitation within the solution space while minimizing the computational burden imposed by the several simulations, the crossover rate (70 % and 95 %) and population size (25 and 50 arrays) were varied. Additionally, to keep a proportionality and an integer number, the elite size varied with the population size, 12 % for cases with 25 layouts and 10 % for cases with 50 layouts. This approach allowed to efficiently explore a diverse range of solutions (while ensuring feasibility) and apply them to other arrangements with more WECs (100 and 200) and larger spacing between WECs (5D and 7D).

The termination criteria were defined based on the stability of the main parameters (q-factor and HRA), with a tolerance of 10^{-4}. This means that the optimization process ends after 20 consecutive generations without relevant changes in the q-factor and HRA *(i.e., within the tolerance of 10^{-4})*.

The arrangement of simulation parameters, including crossover rate, elite size, number of WECs, number of layouts, and minimal spacing between WECs, is detailed in Table 6 - Simulation Setup. These configurations were designed to test the algorithm under different scenarios and evaluate its robustness and performance in optimizing WEC layouts.

3. Data analysis and clustering

As stated previously, the number of sea states significantly increases the computational cost (scaling with population size and generations). Hence, this study prioritizes data reduction through statistical analysis and cleaning techniques avoiding losing data quality and representativeness.

The wave characteristics in the study area were derived from the SIMAR datasets, which are managed by Puertos del Estado. SIMAR provides hourly re–analysis data for wind and wave conditions in the North Atlantic and the Mediterranean Sea, with a spatial resolution of 0.25° × 0.25°. These datasets are generated through a thorough numerical modeling approach that incorporates atmospheric, sea level, and wave conditions [57]. For the specific location of interest, hourly wave data was extracted from the SIMAR dataset, spanning from January 1, 1960 to September 15, 2021. This extensive data set enables a high level of accuracy and reliability. Table 3 present some important parameters.

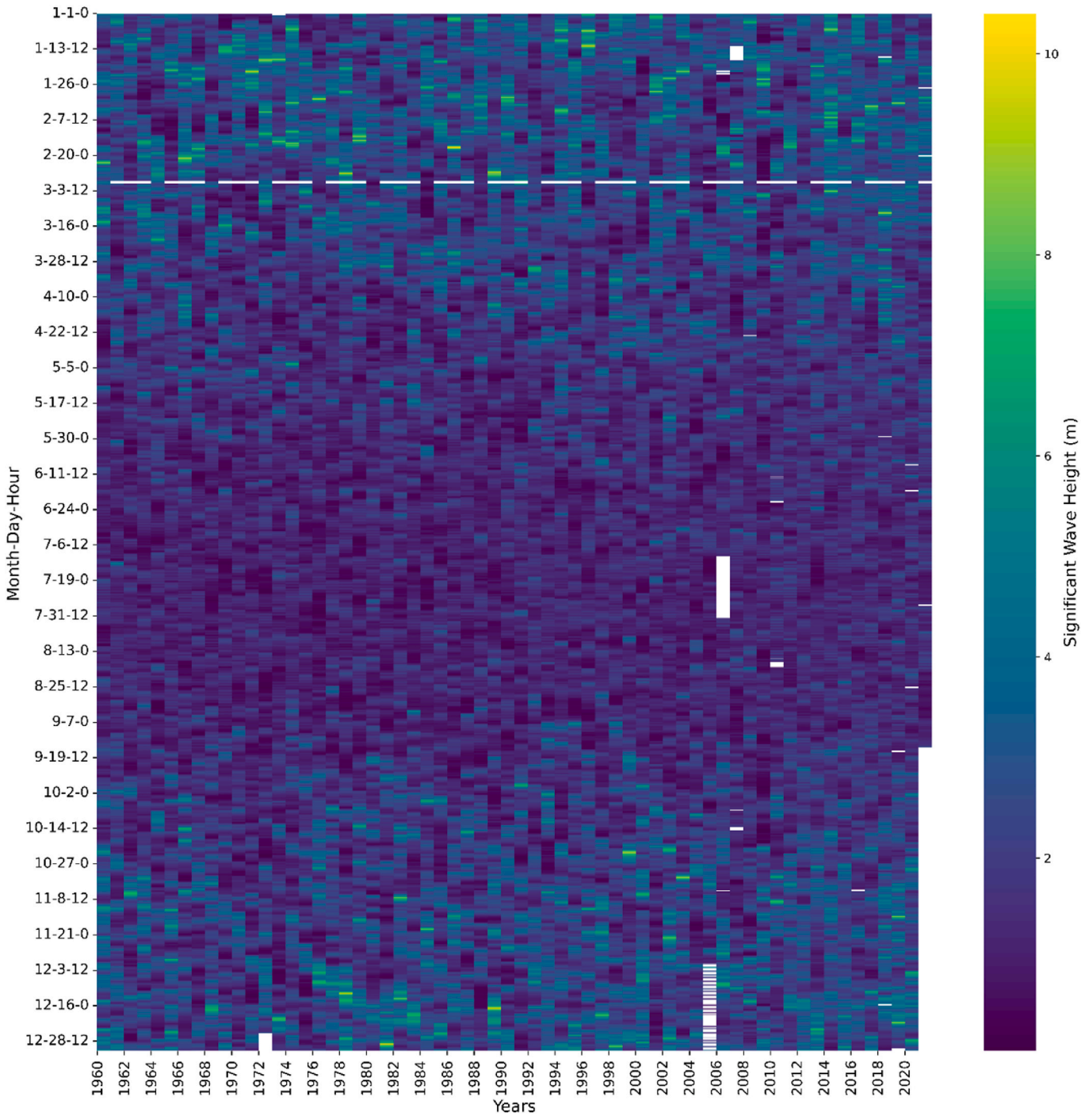

Fig. 8. Heatmap of the significant wave height over time.

Fig. 7 shows the normal distribution of the wave parameters, highlighting the mean and one and two standard deviations (std). As can be seen also in the wave rose, almost all directions are concentrated between incident angles of 225° (WNW) and 327° (NNW). Additionally, the significant wave height (H_S) and the peak wave period (T_P) in the less frequent directions are lower. Fig. 8 presents a heatmap of H_S distribution over time, where is possible to see gaps in the data and a seasonal variation, with lower H_S during summertime.

After the first data analysis, some trials were done with different clustering methods and data cleaning techniques. The three clustering methods presented similar results for the whole dataset (Fig. 9), and for filtering extreme values (Fig. 10), the quantiles 2.5 % and 97.5 % were used. Furthermore, filtering all parameters equally by a top percentile (95th or 99th) yielded similar results, with a slight increase in the directional distribution of clusters. However, there is a significant loss in H_s and T_p data. On the other hand, it is possible to observe that more than 99 % of all incident wave energy is concentrated in directions between 213° and 338°, as shown in Fig. 11, that presents the cumulative distribution of wave power over wave directions.

In the context of this work, WEC farms have the primary goal of harvesting wave energy and protecting the wind farm from high waves. Therefore, the WEC farm does not have to enclose the entire wind farm. Instead, it can be concentrated within an angular range (126° sector), regarding incident wave energy. This range size is particularly

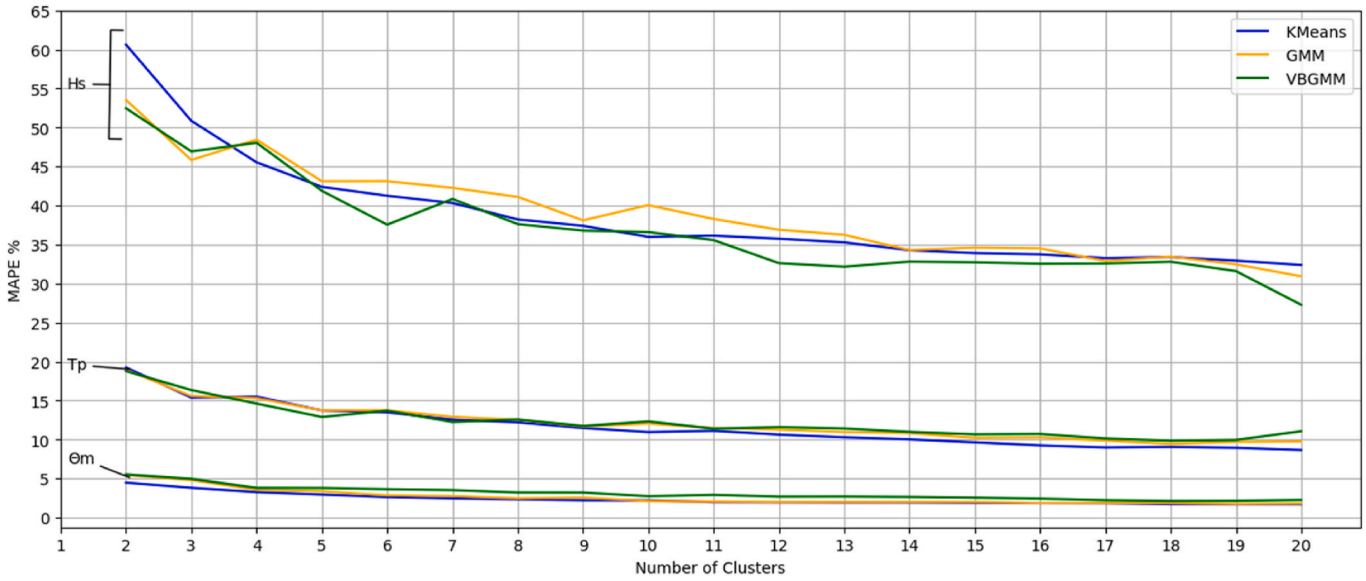

Fig. 9. Mean Absolute Percentage Error (MAPE) for different numbers of clusters and different methods: K–means, Gaussian mixture models (GMM) and variational Bayesian Gaussian mixture models (VBGMM).

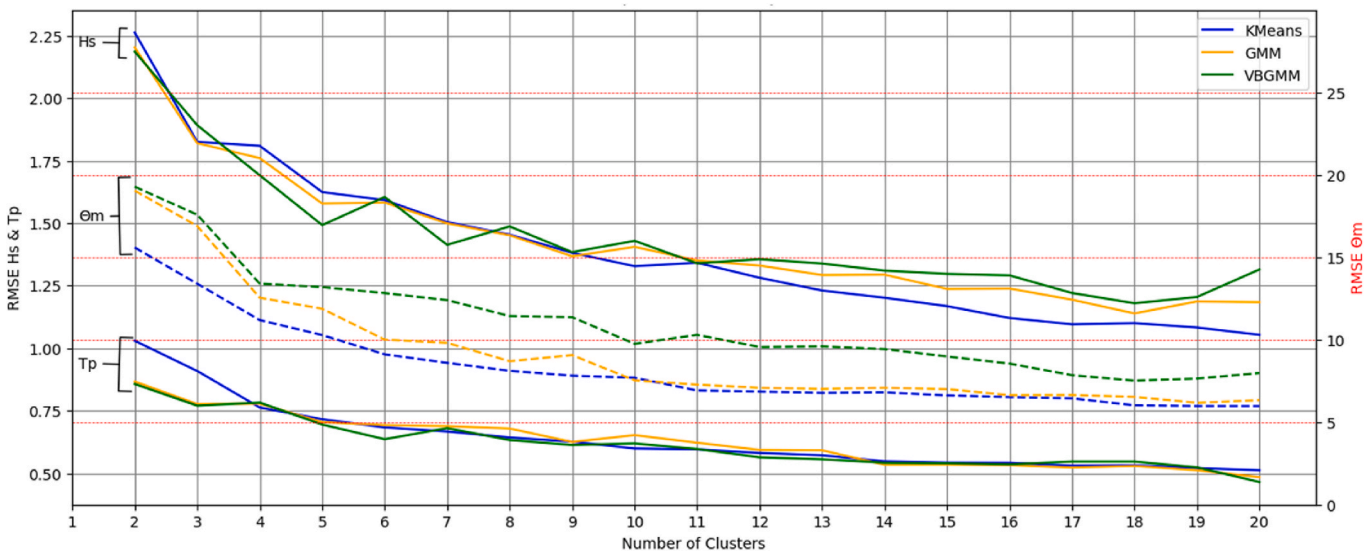

Fig. 10. Root Mean Square Error (RMSE) for different numbers of clusters and different methods: K–means, Gaussian mixture models (GMM) and variational Bayesian Gaussian mixture models (VBGMM).

important because traditional distance metrics, like the Euclidean distance used in k-means clustering, do not handle angular distances well. For instance, they might calculate the distance between 10° and 350° as 340° instead of the correct 20°, which is essential for circular distance considerations. This highlights the need for specialized methods or adjustments in clustering algorithms to handle circular distance calculations effectively.

Upon implementing a cleaning over the directions, keeping only the 126° sector between 213° and 338°, the data was subjected to clustering once more, to determine which number of clusters could provide sea states that represent at least 90 % of the incoming wave energy. In this process, power representativeness (φ_p) was used,

$$\varphi_p = \frac{\sum_{c=1}^{n} (P_{centroid} \times N_c)}{\sum_{i=1}^{N} P_i} \tag{4}$$

where $P_{centroid}$ represents the wave energy per wave front for each sea state, represented by the centroid of the cluster, N the total number of data values, N_c the values inside a cluster, n the number of clusters, and P_i the incoming wave energy per wave front for each data value. Fig. 12 shows the outcomes of the cluster's representativeness map up to 20 clusters. Notably, the partition in 8 clusters is the lowest partition where the rate of power efficiency surpasses 90 %. Hence, it was determined that 8 clusters were the minimum number required to effectively represent the sea states.

Fig. 13 shows the data obtained by the directional filtering, clustered by the k–means. The centroids of each cluster represent the wave parameters that were pursued (shown in Table 4).

An automated search was conducted within the dataset, assessing MAPE of each sea state in relation to the hourly mean of each parameter. This analysis aimed to locate the optimal temporal positioning throughout the year for these sea states. The findings demonstrate that selected sea states effectively encapsulate the seasonal variations across

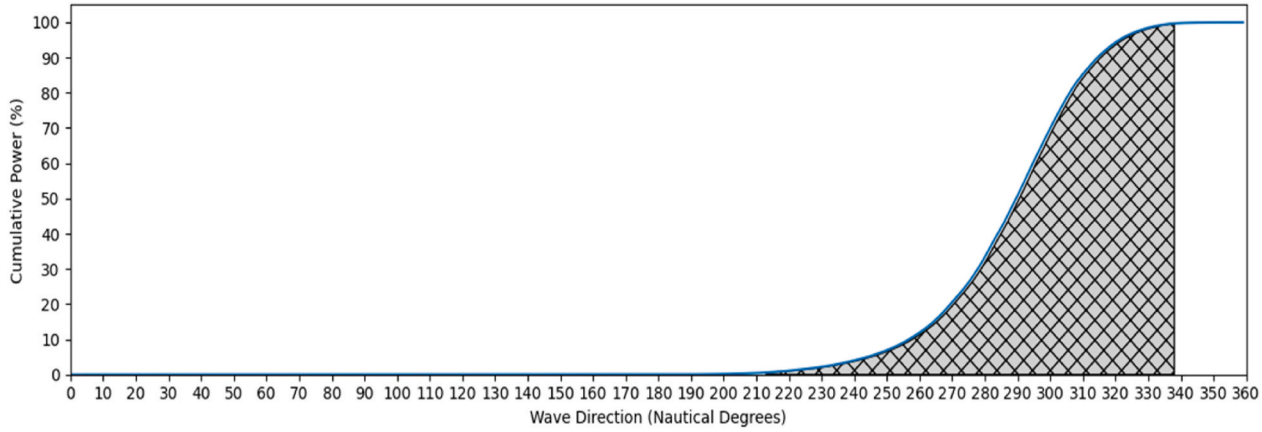

Fig. 11. Cumulative incident wave energy distribution by wave direction.

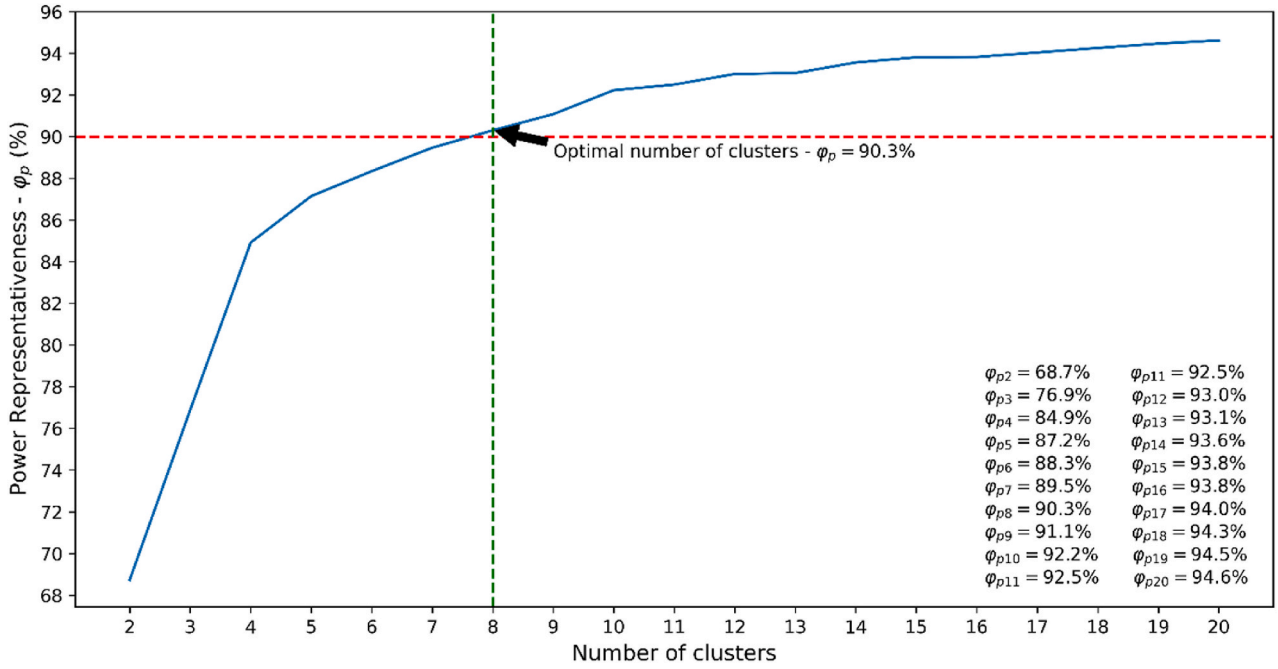

Fig. 12. K-means clustering wave power efficiency up to 20 clusters.

the entire annual cycle (Fig. 14).

4. Wave farm layout optimization

4.1. Definition of single WEC power absorption

The definition of power absorption of a single WEC is important to estimate the *q-factor*, which is the most used parameter for the optimization of wave energy farms. Since using the rated power of the device overestimates the power output, two different methods were used to estimate the average power absorption of a single WEC: positioning of the WEC randomly a thousand times in the domain, and in an arc path with each WEC at every 0.5°. As the average of the arc method returned a higher single WEC absorption, this method was used to estimate the *q-factor* of the layouts. The statistics of the arc method are displayed in Table 5.

4.2. Simulation setup

The crossover rate and the population size have a significant influence on the model computational time. Therefore, the used approach commenced with a series of simulations where these parameters were systematically varied. Then, upon identifying the optimal configuration, further simulations were conducted to assess the method's efficacy across a broader spectrum, encompassing a larger array of devices and increased inter-device spacing.

Table 6 provides a comprehensive overview of the simulation setups employed in this investigation, detailing the average new layouts generated (referred to as "children") and the corresponding number of simulations needed by each variation of the GA parameters. The "efficiency" of each simulation iteration was quantified by computing the average execution time across its generational iterations, compared against the baseline established by the fastest simulation, which was S1.

As will be more comprehensively elaborated in section 4.3, simulation S1 was not only the fastest (by generation) but also presented the best results. Hence, the simulations denoted as S5 to S8 aimed at elucidating the method's scalability to accommodate a larger number of WECs and increased inter-WEC spacings, using as basis S1 configuration. This configuration entailed a crossover rate set at 70 %, a population size consisting of 25 individuals (farm layouts), and an elite rate of 12 %

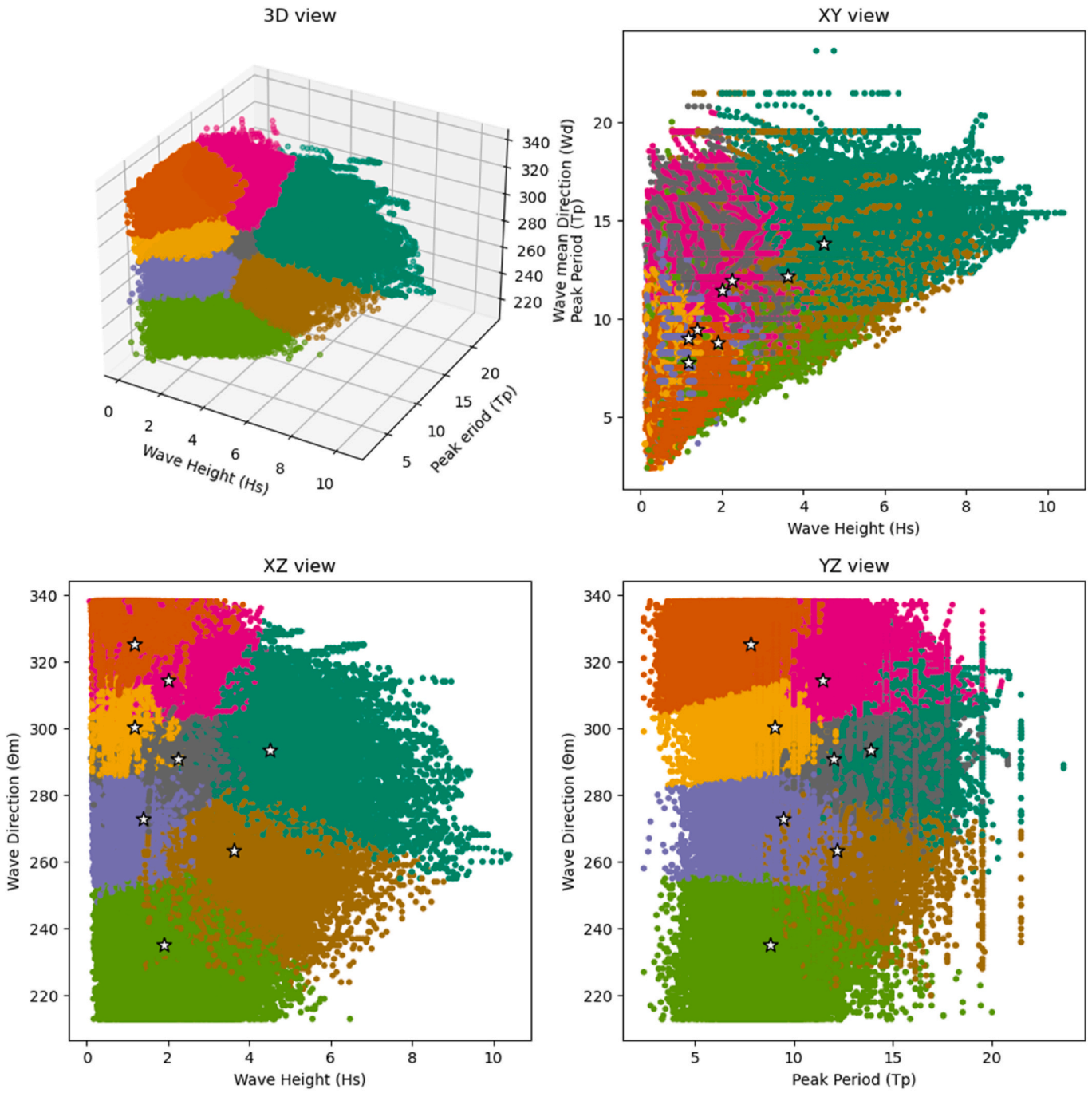

Fig. 13. – Clusters obtained by K–means. Each color represents one cluster and the white stars the centroids. (For interpretation of the references to color in this figure legend, the reader is referred to the Web version of this article.)

Table 4
Wave parameters achieved with k–means.

Cluster	Hs (m)	Tp (s)	Θm (°)
0	1.2	7.8	325.5
1	1.2	9.1	301.5
2	1.3	9.4	274.7
3	1.9	8.8	235.7
4	2.1	11.6	314.1
5	2.3	12	290.7
6	3.5	12	262.7
7	4.6	13.9	292.2

(equivalent to 3 individuals). Notably, the average efficiencies observed in these subsequent simulations deviated by less than 1 % from that of the benchmark S1 simulation.

In order to validate the proposed method and verify the accuracy of the algorithm, additional simulations were performed using the simulation setups S1, S5 and S6 as base because they are the ones that have a different number of WECs. The additional simulations vary the weights associated to wave protection and power production. Three scenarios are considered: i) same weight for both objectives, as in the previous setups (s = p), and only one objective function is optimized, for (ii) maximum power production (p = 1) or (iii) maximum wave protection (s = 1).

The simulations were executed on the FEUP cluster, which comprises

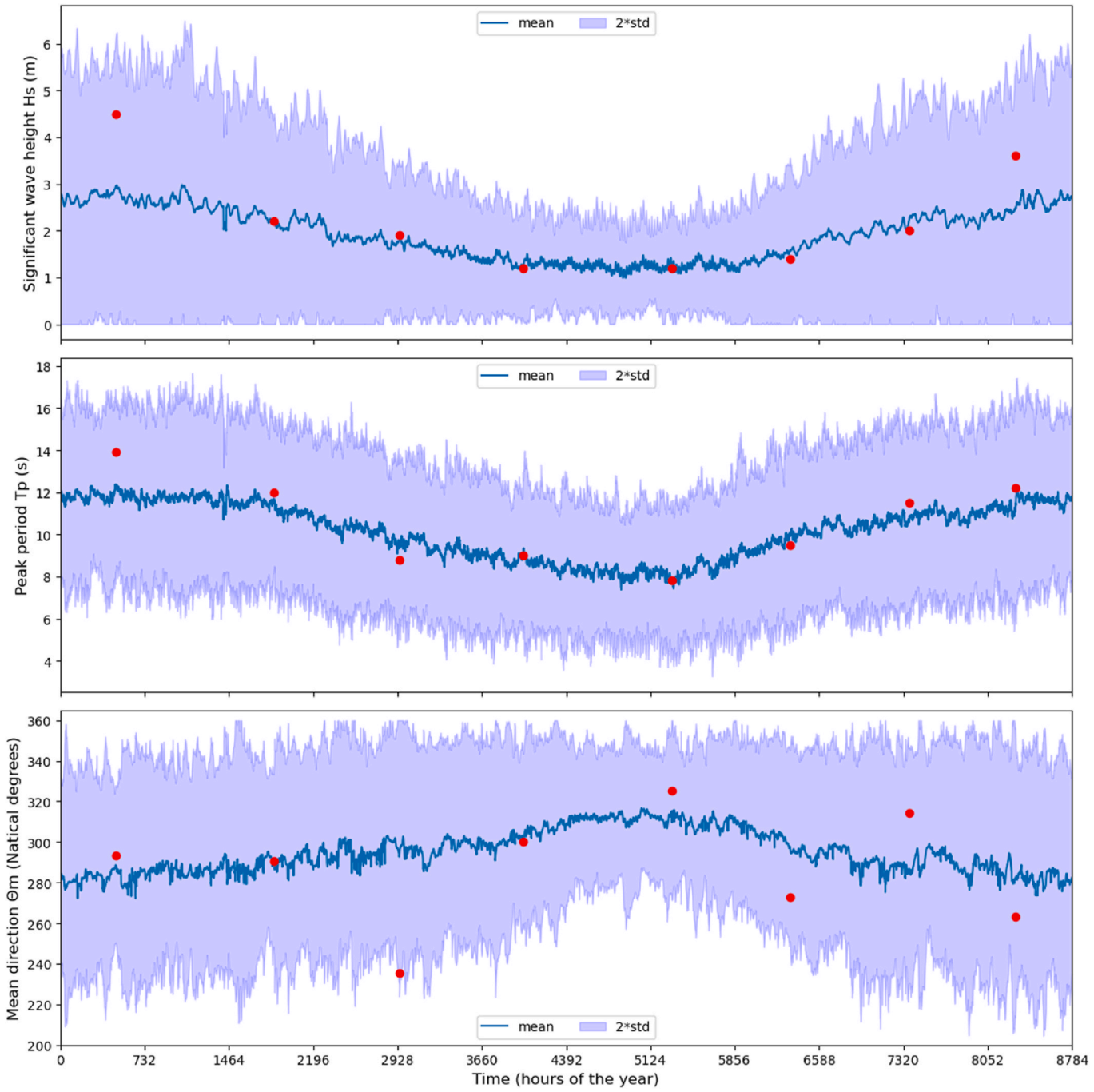

Fig. 14. Fit of the chosen sea states compared with hourly mean parameters. Blue line is the hourly mean and the purple shadow the standard deviation multiplied by 2, which represent approximately 95 % of data. (For interpretation of the references to color in this figure legend, the reader is referred to the Web version of this article.)

Table 5
Statistics of the single WEC simulations using the distribution in arc.

Parameter	Value (kW)
mean	129.3
std	9.6
min	104.6
25 %	120.6
50 %	130.3
75 %	135.3
max	149.3

multiple nodes, each possessing distinct CPU processing capacities. To ensure equitable comparison, the number of generations for each simulation was estimated to achieve at least the computational execution time equivalent of 100 generations of the slowest simulation (S4), which was about 4 days. It is noteworthy that, to maintain consistent runtime conditions, all simulations were executed utilizing 24 cores on an AMD EPYC 7443 processor for a minimum of 10 generations. Consequently, owing to its superior performance, the S1 simulation was extended to 500 generations to optimize the layout of the WEC farm layout.

Table 6
Simulation setup.

SIM	WECs	Layouts	Min Dist.	Elite	Crossover Rate	Children/Generation	Simulations/Generation	Max Gen.
S1	50	25	2.5D	0.12	0.70	15.4	123.2	500
S2	50	25	2.5D	0.12	0.95	20.9	167.2	260
S3	50	50	2.5D	0.10	0.70	31.5	252.0	150
S4	50	50	2.5D	0.10	0.95	42.75	342.0	120
S5	100	25	2.5D	0.12	0.70	15.4	123.2	200
S6	200	25	2.5D	0.12	0.70	15.4	123.2	200
S7	50	25	5D	0.12	0.70	15.4	123.2	125
S8	50	25	7D	0.12	0.70	15.4	123.2	125

Table 7
Results of S1, S2, S3 and S4 simulations regarding the average execution time.

SIM	Average generations time (min)	100 generations time (days)	Generations in 4 days	Run time efficiency
S1	18.5	1.3	308	1
S2	25.1	1.7	227	1.36
S3	37.8	2.6	150	2.05
S4	51.3	3.6	111	2.78

4.3. Results of the wave farm layout optimization

The study initially focused on optimizing the parameters of the GA, contrasting the runtime efficiency and the evolution of results for HRA, *q-factor*, and WLA across generations and execution time. Table 7 summarizes the outcomes derived from using 24 cores within the AMD EPYC 7443 node. It delineates the average execution time for 1 and 100 generations, estimates the equivalent generations attainable within a four-day timeframe, and provides the runtime efficiency of each simulation.

The evolution of the results is presented in Fig. 15 for the HRA and *q-factor*, and in Fig. 16 for the WLA, offering comparisons across generation and execution time. Upon individual examination, all simulations exhibit remarkably similar trends across generations, with S4 showing marginally superior results compared to the others.

In comparing simulations S1 to S4 using the WLA index, it becomes evident that by the generation, S4 notably distinguishes itself from the others. This outcome was anticipated, given the utilization of a 95 % crossover rate and a larger population, both of which contribute to a more favorable environment for the emergence of novel and superior individuals. However, it is crucial to acknowledge that the assessment of farm layouts depends on SWAN simulations, and expanding both parameters leads to an increase in the number of simulations and, subsequently, the execution time. Consequently, the optimal adjustment for the algorithm must carefully weigh against execution time constraints. In this context, simulation S1, the swiftest among them, unequivocally demonstrates superior results with the best balance between HRA and *q-factor* from the initial hours of simulation.

Table 8 shows the results of the simulations considering the execution time of 100 generations of S4, which is 86 h. The data show that as it is a multi-objective optimization, and both parameters are equally balanced, the best result for one parameter will not always return the best output. As an example, in Fig. 16 the results of WLA for S3 after 86 h are better than for S2 and S4, although S2 has a higher *q-factor* and S4 has a higher HRA than S3.

Having established the S1 configuration as the optimal choice, simulations S5 to S8 were subsequently conducted to gauge the algorithm's performance across other variants. These included variations in the number of WECs and in the minimal distance between them. By exploring these additional factors, we aimed to comprehensively assess the adaptability and efficacy of the GA in accommodating different parameters crucial to the design and optimization of WEC farm layouts.

All simulations performed showed a distinct evolutionary trajectory, even when sharing identical array parameters. The individual progressions across generations are visually depicted in Fig. 17, where a simultaneous moving average, with a window of 5 values for both objectives (HRA and *q-factor*), is presented for all simulations. Fig. 17 provides an interesting visualization of the trade-offs between the objectives. Furthermore, Fig. 18 offers insight into the optimized final WEC farm design for each variation. Despite all simulations showcasing a heightened density of WECs strategically positioned to harness the most

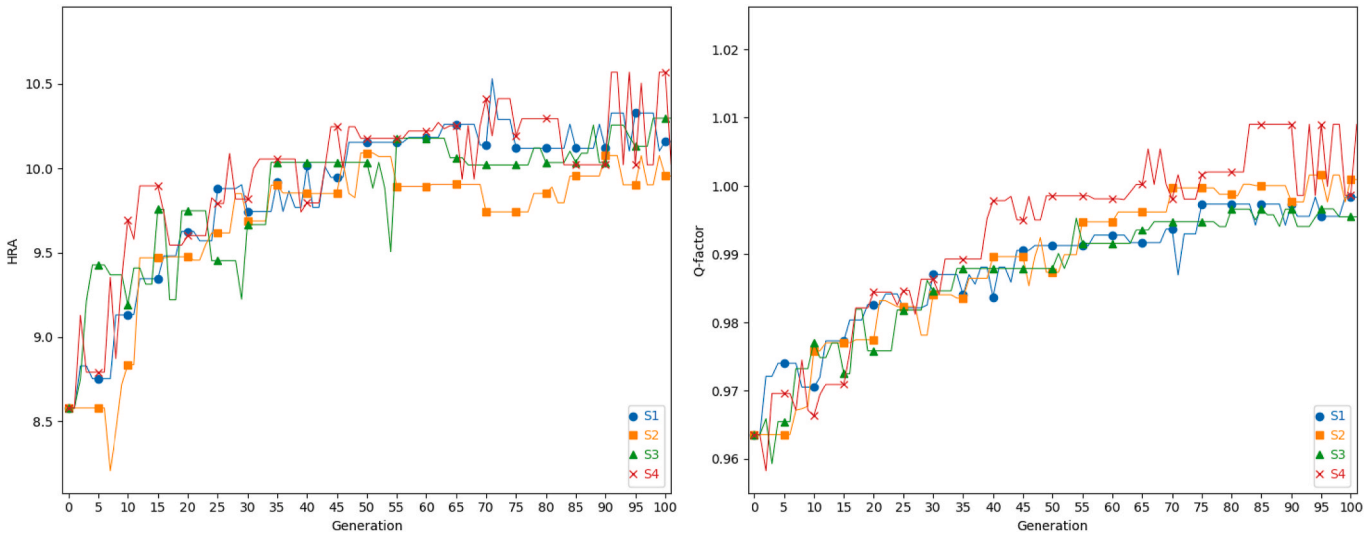

Fig. 15. Evolution of the parameters HRA (left) and q-factor (right) of simulations S1 to S4 through 100 generations.

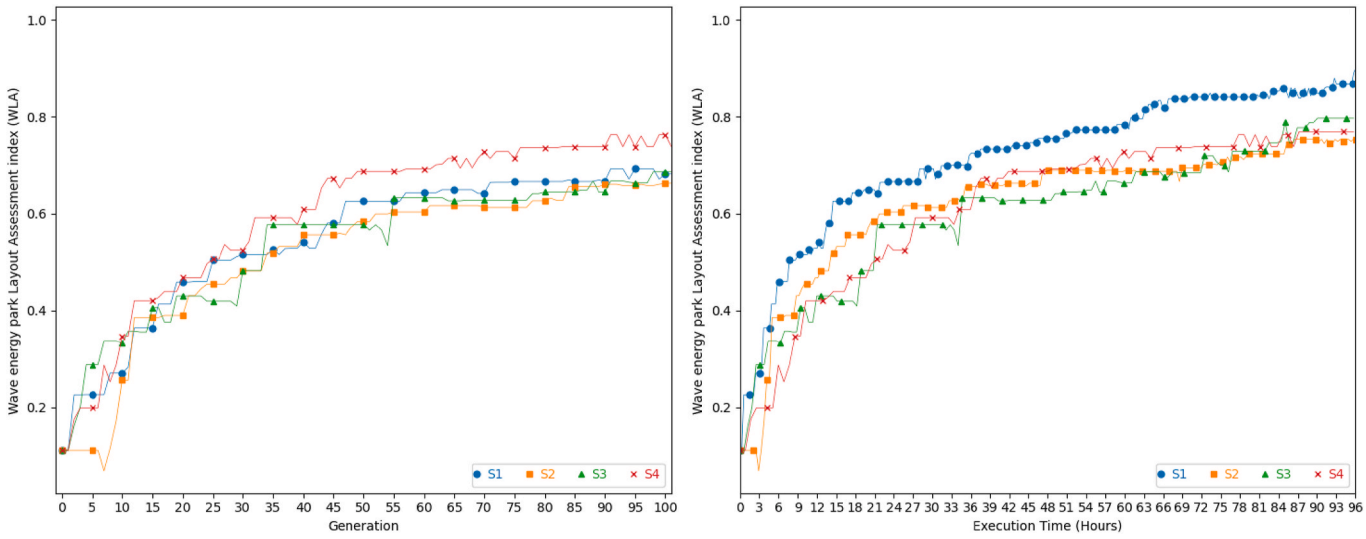

Fig. 16. Wave energy park Layout Assessment index (WLA) evolution of simulations S1 to S4, comparing the result by generation and the execution time.

Table 8
Results of simulations S1, S2, S3 and S4 considering an execution time equivalent of 100 generations of S4 (86 h).

Simulation	Generations	HRA (%)	Q-factor
S1	279	13.21	1.008
S2	205	12.28	1.010
S3	136	12.44	1.007
S4	100	12.93	0.999

energetic sea states, the path to achieving these outcomes varied significantly, resulting in diverse final configurations. These graphical representations underscore the nuanced and multifaceted nature of the optimization process, highlighting the unique pathways each simulation traverses to attain its final objective.

In the analysis of the different arrangement's inputs and restrictions, the evolution of all simulations was plotted considering the values of HRA and *q-factor*, in Fig. 19, and of WLA, in Fig. 20. The dynamic nature of the WLA requires recalculating it after every generation, as the data is normalized. To ensure consistency across simulations, the WLA for all scenarios was calculated using the global maximum and minimum values derived from simulations S1 to S4 (in Fig. 16) and simulations S1 to S8 (in Fig. 20). This approach facilitates a standardized comparison across different simulation runs, allowing for a comprehensive evaluation of the optimization process's performance and effectiveness.

The exceptionally high HRA value in the 200 WECs layout (S6) resulted in a significantly larger WLA, effectively compensating for its lower *q-factor*. However, it is crucial to acknowledge the challenges posed by area restriction issues arising from either an excessive number of WECs or a wide inter-WEC spacing. These constraints constitute formidable obstacles within the optimization framework, as they can limit the development of the algorithm, causing premature convergence evidenced by horizontal curves. This underscores the complex interplay between the layout optimization objectives and the physical constraints inherent in the wave energy conversion domain.

Table 9 presents the final outcomes of each simulation. Although comparisons among simulations S1 to S4 are not feasible due to the different execution times and generation counts, it is pertinent to note that comparisons between S5 to S6 and S7 to S8 are viable, as these simulations are variations of the same parameter and feature identical generation counts. Additionally, and in accordance with the findings presented in Ref. [14], the accessibility for the operation and maintenance of the wind farm emerges as a critical parameter for analyzing the efficiency of wave height reduction. Consequently, this parameter has been duly incorporated into Table 9 for a comprehensive analysis.

In contrast with the findings detailed in Ref. [14], which share the same inputs as this study and entailed the positioning of 4 WEC farms in a customized arc arrangement, simulation S1 exhibited notable superiority. Specifically, in comparison to the best layout identified in Ref. [14], simulation S1 showed an 87 % improvement in absorbed wave power and a 46 % enhancement in wave height reduction within the designated area of interest.

As the S1 simulation demonstrated superior performance, extending it to 500 generations allowed for a detailed analysis of its behavior. Fig. 21 shows a notable initial improvement in both parameters, followed by a gradual enhancement in *q-factor* over the subsequent generations, while HRA remains relatively stable after 300 generations. This pattern highlights the inherent trade-offs between parameters, notably observed in the best fit curve, where new individuals with higher *q-factor* exhibit lower HRA than the previous best fit, and *vice versa*.

The Capture Width Ratio decreases as the number of WECs increases, indicating a trade-off between total energy absorption and individual device efficiency. Simulations with fewer WECs, such as S1 (50 WECs) and S2 (50 WECs), show higher CWR values (40.25 and 39.62), reflecting better energy capture efficiency per device. However, as more WECs are added, like in S5 (100 WECs) and S6 (200 WECs), the CWR drops significantly, despite a higher total power absorption, suggesting that scaling up the number of devices reduces their relative efficiency. This trend highlights the balance between optimizing the number of devices and maximizing energy capture efficiency.

Moreover, it is noteworthy that not only the best fit individual or the elite evolve. Instead, the entire population experiences an increase in values, indicating a collective trend toward achieving optimal results. While the population range maintains the potential to circumvent local optima, the ongoing evolution of individuals across successive generations suggests a continual exploration of the solution space, thus mitigating the risk of convergence towards suboptimal solutions.

Interestingly, the best fit individual remained unchanged in the last 50 generations, despite sporadic instances of improved HRA and *q-factor* in other individuals. This suggests the possibility of a superior fit individual, albeit with diminishing probability as the best fit remains unchanged over successive generations.

4.4. Comparative analysis and validation of the optimization algorithm

A comparative study was conducted to validate the performance and accuracy of the proposed optimization algorithm. This section presents a

Fig. 17. Comparison of the evolution of the HRA and q-factor parameters for all simulations carried out.

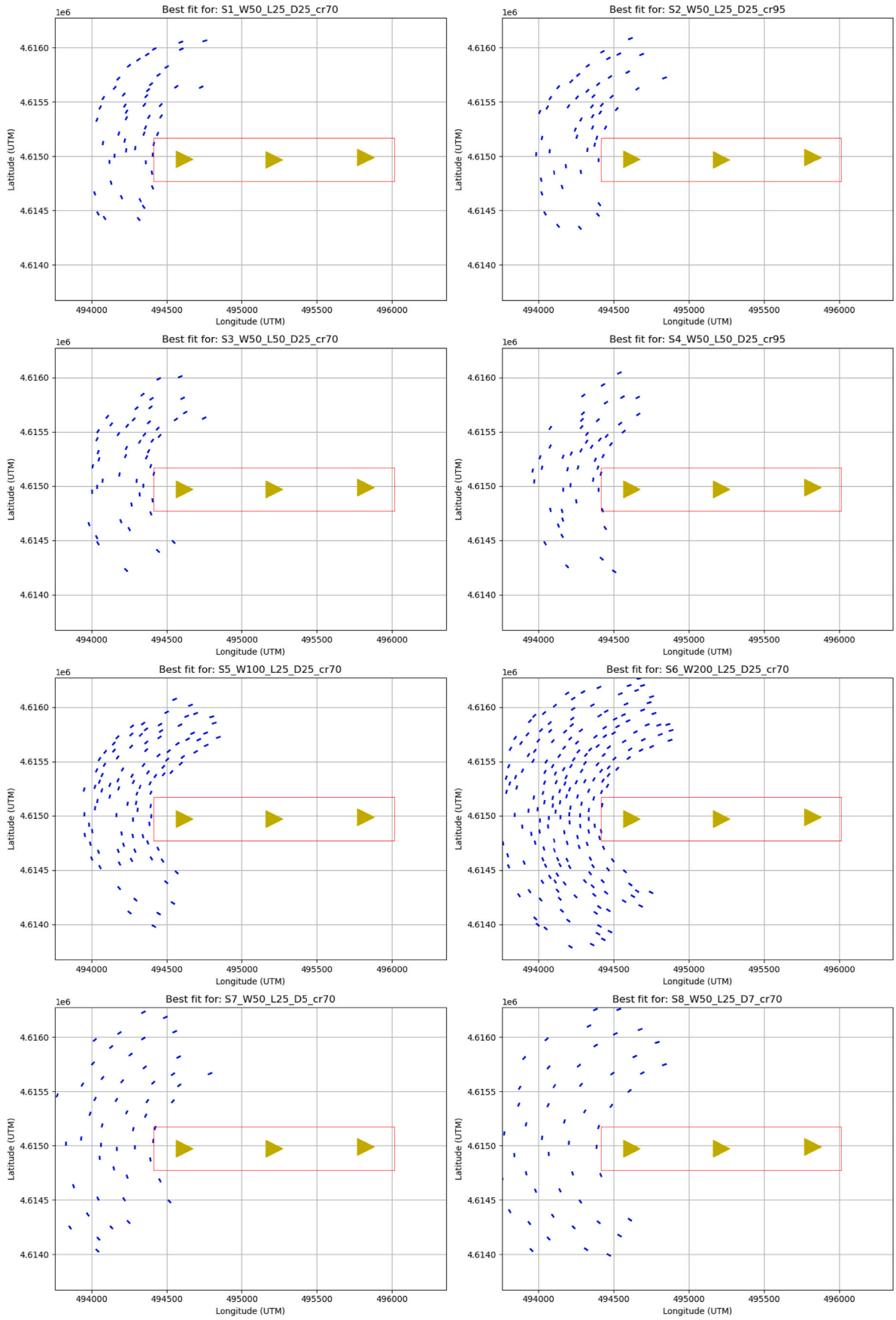

Fig. 18. Best fit layout for each simulation. The blue lines represent the WECs, the yellow triangles the wind turbines of the WindFloat Atlantic and the red rectangle the interest area. (For interpretation of the references to color in this figure legend, the reader is referred to the Web version of this article.)

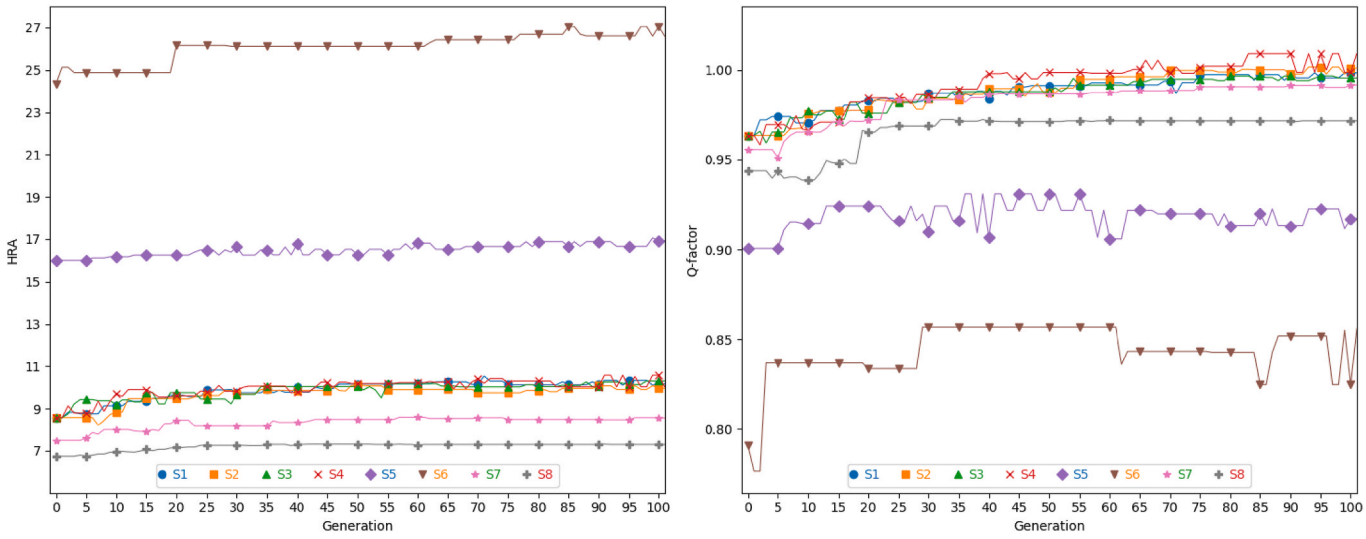

Fig. 19. Evolution of the parameters HRA (left) and *q-factor* (right) of all simulations through 100 generations.

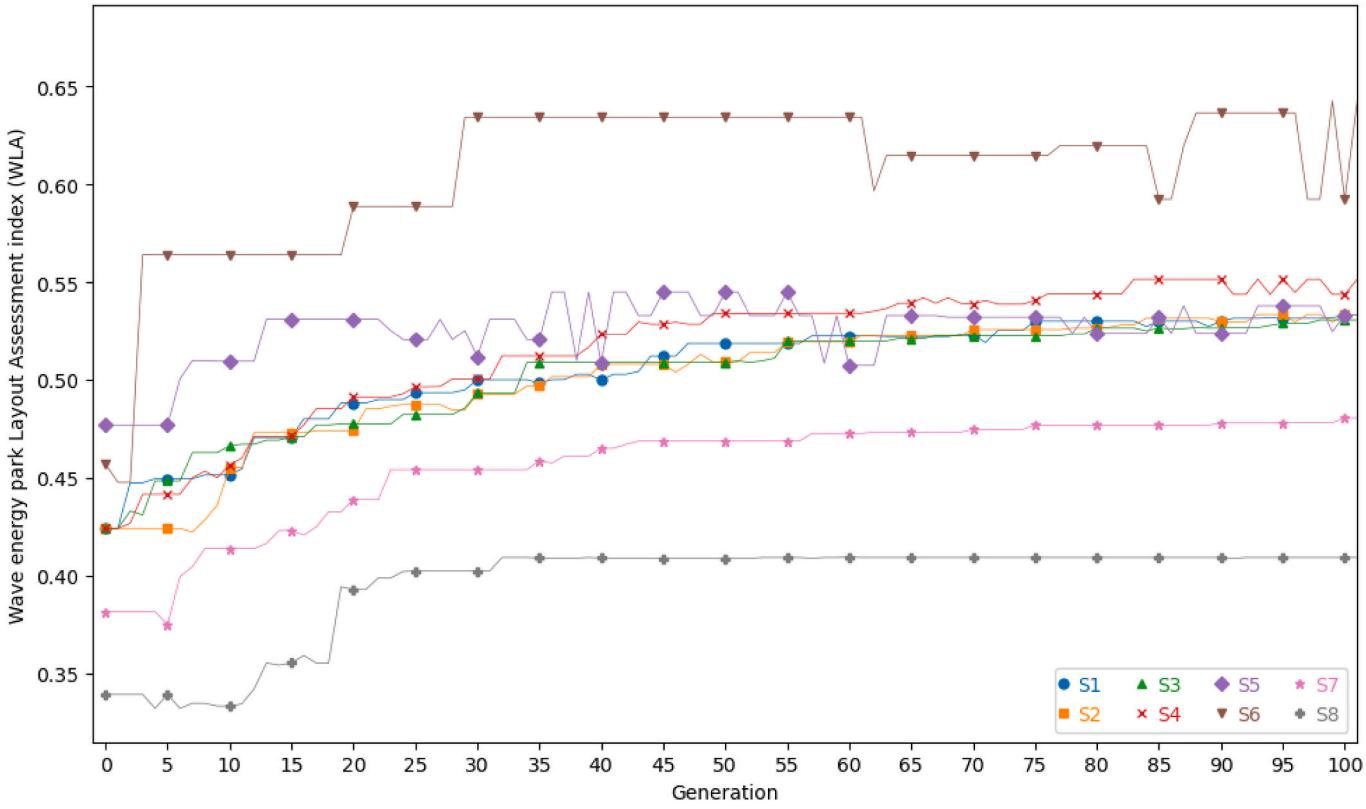

Fig. 20. Wave energy park Layout Assessment index (WLA) evolution of all simulations comparing the result by generation and the execution time.

Table 9
Final generation results for best fit layout, and estimated increase in the accessibility of the wind farm for operation and maintenance.

Simulation	Generation	Power absorption (MW)	CWR	Q-Factor	HRA (%)	Accessibility increase (%)
S1	500	33.07	40.25	1.023	13.21	28.4
S2	260	32.71	39.62	1.012	12.52	26.7
S3	150	32.52	33.21	1.006	12.82	27.6
S4	125	32.36	38.96	1.001	12.86	27.8
S5	200	59.77	34.39	0.924	21.08	44.0
S6	200	221.53	30.08	0.857	32.14	69.5
S7	125	32.12	38.90	0.992	10.43	22.2
S8	125	31.41	38.27	0.972	8.92	19.0

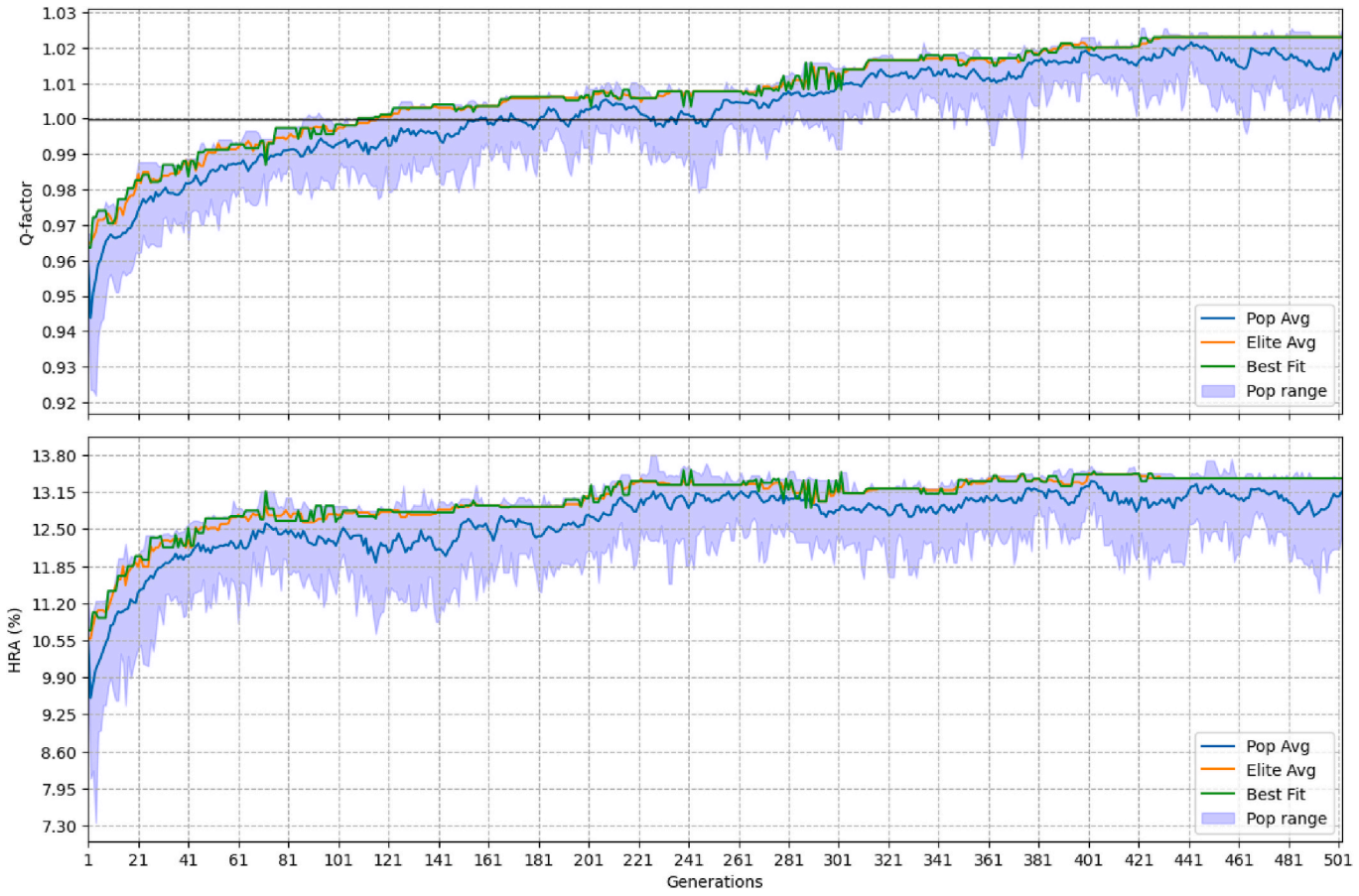

Fig. 21. Evolution of simulation S1 for the HRA and *q-factor* parameters. The purple shadow represents the range of values presented in the population, the green line the best fit layout, the blue line the average of all population and yellow line the average of elite layouts. (For interpretation of the references to color in this figure legend, the reader is referred to the Web version of this article.)

Table 10
Results of the verification and validation study. Where Δd is the distance from the first run position.

Sim	Power abs (MW)	Power Error (%)	HRA (%)	HRA Error (%)	Layout RMSE	Pairs (%) Δd >1D	Centroid Δd (m)
S1 rerun	6.53	0.26	12.63	−1.80	112.71	52	16.76
S5 rerun	11.90	−0.47	20.89	−0.91	106.81	57	22.16
S6 rerun	22.17	0.09	32.48	1.04	98.81	44	14.42
S1 max shield	6.22	−4.42	14.53	12.96	225.71	86	51.55
S5 max shield	11.44	−4.28	22.76	7.95	136.52	88	68.36
S6 max shield	21.24	−4.14	33.97	5.68	110.52	88	49.73
S1 max power	6.59	1.20	9.78	−23.97	336.69	90	171.72
S5 max power	12.09	1.14	18.94	−10.14	180.73	91	84.68
S6 max power	22.35	0.88	30.43	−5.32	170.28	93	72.00

detailed analysis of three selected cases with a different number of WECs (S1, S5, and S6). This study compares optimization results obtained using the dual-objective function (WLA) against those obtained with single-objective functions focused exclusively on maximizing the power production (Q-factor) and the wave protection factor (HRA). This comparison aims to highlight the importance and effectiveness of the dual-objective approach.

Additionally, the accuracy of the algorithm is evaluated by rerunning the selected cases and comparing the optimized layouts with those presented in Fig. 19 of the original manuscript. To evaluate the positional discrepancies between the rerun optimized layouts and the original simulation, the RMSE was employed as a quantitative metric. The calculation methodology comprised two key steps.

First, to find the optimal pairing of WEC positions, the Kuhn-Munkres algorithm was utilized to establish the optimal correspondence between the WECs in the original and rerun layouts. This method minimizes the total positional distance across all WECs, ensuring an objective and globally optimal pairing. Once the optimal pairs were identified, the RMSE was calculated to the distances between the paired WECs. This approach captures the magnitude of the average positional error in meters, providing a comprehensive measure of the layout deviations between simulations. Furthermore, the number of WECs whose positions changed more than the WECs width was accounted, to evaluate the precision.

This methodology ensures a rigorous and systematic assessment of the optimization algorithm's consistency. The RMSE serves as a robust indicator of the accuracy of the rerun layouts compared to the original simulation, reflecting the algorithm's capability to reproduce optimal configurations under varying conditions.

Considering the computational costs, all simulations performed for

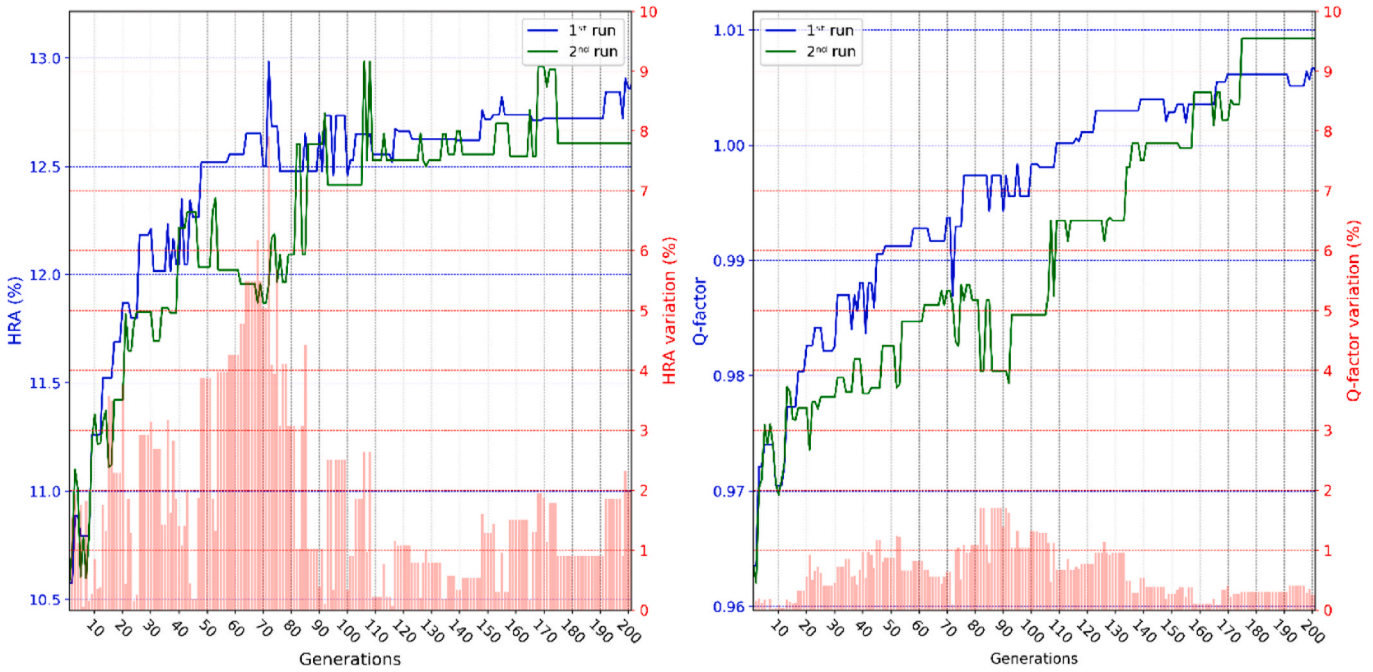

Fig. 22. Comparison of the evolution of the HRA and q-factor values and it their variation for the two simulations with S1 parameters. The blue line represents the evolution of first run, the green line the evolution of second run and the red bars represents the percentual difference between each run. (For interpretation of the references to color in this figure legend, the reader is referred to the Web version of this article.)

verification were run with a termination criterion of 200 generations and their results compared to the results of the original simulation at the same generation. The outcomes for the 200th generation of configurations S5 and S6 are presented in Table 9 (for reference, configuration S1 achieved a power absorption of 6.51 MW and an HRA of 12.86 % after 200 generations). A summary of the results for all cases can be found in Table 10.

To further illustrate the findings, the outcomes of the S1 configuration are highlighted in Fig. 22, which provides an evolutionary comparison of the two optimization runs with equal weights assigned to power absorption and shield protection. Additionally, Fig. 23 showcases the layouts of all S1 simulations, including those optimized solely for power absorption and wave protection. These visualizations emphasize the versatility and effectiveness of the proposed optimization algorithm under varying objectives.

The second round of simulations with equal weights assigned to wave protection and power absorption produced results that were remarkably similar to the first ones. Approximately half of the WECs were positioned in locations less than one device diameter (<1D) apart, with variations in HRA of less than 2 % and power absorption differing by less than 0.5 %. Additionally, the RMSE remained stable around 5D across all three simulations of different numbers of WECs. The evolutionary process of the optimization was also highly similar, indicating a strong tendency toward convergence on a global optimum with minimal variation.

Notably, the simulations performed for maximizing just one parameter exhibited higher variations in RMSE and centroid positions compared to the rerun simulations, as these focus on a single objective, which causes greater layout variability, with approximately 90 % of the devices repositioned. The RMSE was higher for layouts with fewer WECs compared to those with more devices. A plausible explanation is the reduction of available space for positioning in larger layouts, which leads to a more uniform device distribution and minimizes the average positional differences between optimized pairs.

The centroids, which can represent the positioning of a central collecting hub, were highly stable for the rerun simulations, with variations of 1D or less. An exception occurred in the S1 maximum power case, where centroid variation reached 8D due to the focus on maximizing power absorption alone, which led to more distinct optimized positions. Nevertheless, considering the layout domain of approximately 1.3 km^2, this difference is practically insignificant.

The random nature of the initial generation and the mutation process, which allows WECs to be repositioned anywhere within the domain regardless of previous layouts, supports this global optimization search. This tendency for the simulations to converge toward a common solution is further demonstrated by the evolution of the entire population, as shown in Fig. 21, where the population progresses collectively toward an optimal configuration.

These results further corroborate the trend toward an optimal global layout. A plausible explanation for the consistency of results and the similarity in evolutionary paths, even when considering continuous spatial positioning, lies in the random sampling of 500 layouts in the initial generation. This broad exploration minimizes the likelihood of convergence to local optima by effectively distributing the WECs across the entire domain.

For the simulations that aimed to maximize only one parameter in the objective function, the non-prioritized parameter was consistently neglected in the best-fit solutions, never achieving the highest value in the generation and remaining close to the generation average. Conversely, the prioritized parameter was always maximized. This is reflected in Table 10, where reductions in power absorption and HRA are evident for the neglected objectives.

Interestingly, Table 10 also reveals that, even with equal weights, power absorption reaches levels very close to those achieved in simulations exclusively maximizing power. This suggests a potential barrier for this parameter, as the q-factor is already close to or exceeds 1. On the other hand, HRA appears to have more room for improvement. Furthermore, small variations in power absorption have a more pronounced impact on wave protection than variations in protection have on power absorption.

Examining Fig. 23 and the variations in centroids, it becomes evident that prioritizing one objective significantly influences the spatial arrangement of the layouts. Simulations that prioritize wave protection exhibit a more compact spatial distribution, concentrating the WECs in

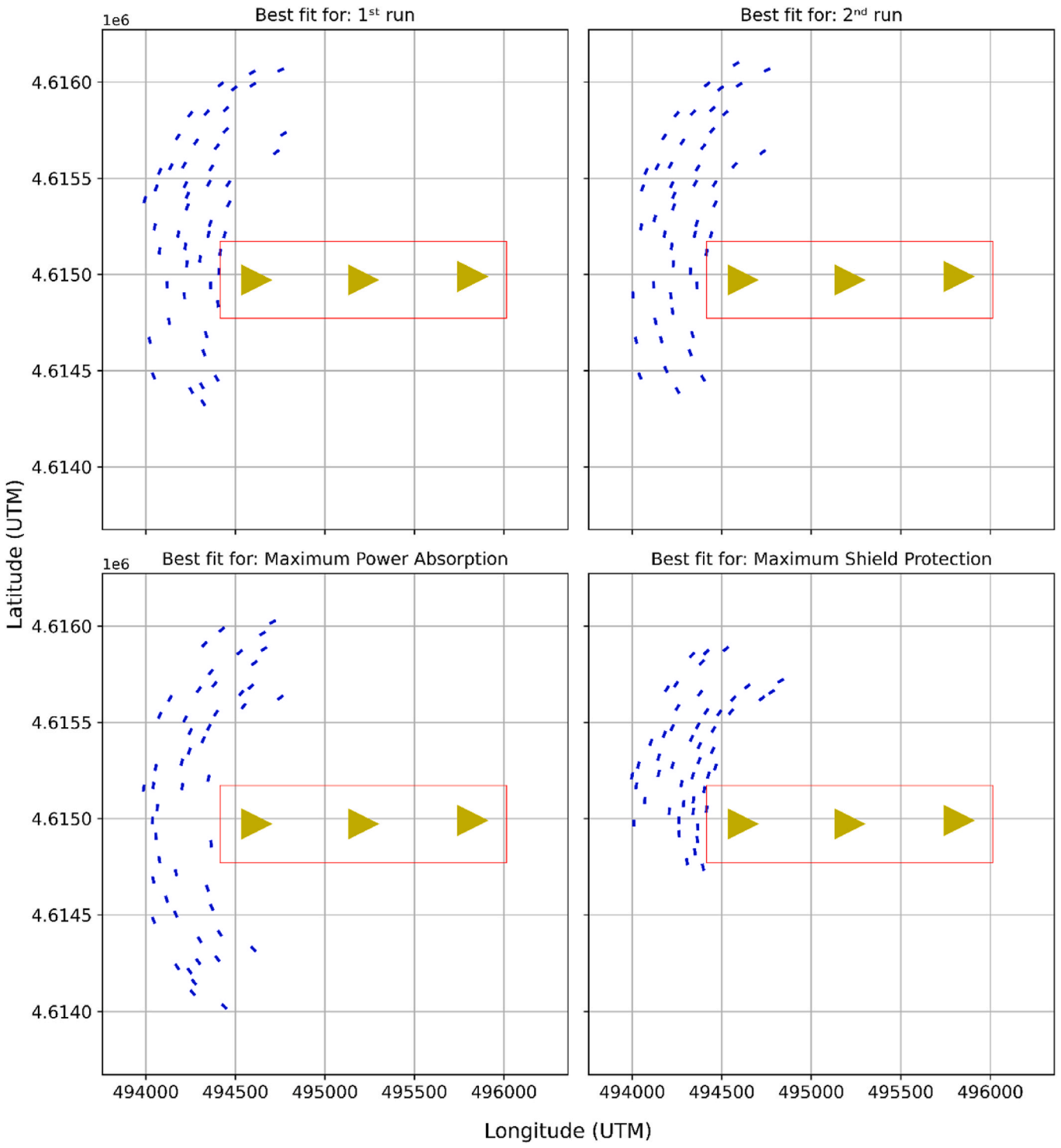

Fig. 23. Best fit layout of generation 200 for each simulation using the S1 parameters. The blue lines represent the WECs, the yellow triangles the wind turbines of the WindFloat Atlantic and the red rectangle the interest area. (For interpretation of the references to color in this figure legend, the reader is referred to the Web version of this article.)

areas aligned with the predominant wave energy directions and frequencies. Conversely, simulations that prioritize power absorption result in a more dispersed spatial configuration, aimed at minimizing interference between WECs and maximizing wave energy exposure for each device. These findings highlight how the objective function weights influence not only the performance metrics but also the spatial characteristics of the optimal WEC layouts.

These findings emphasize the importance of carefully calibrating the weights of the objective function. Their adjustment should be based on thorough evaluation and may consider a range of economic, social, and environmental factors to reflect stakeholder priorities and optimize outcomes effectively.

5. Conclusions

This study successfully employed a GA to optimize the layout of a

WEC farm situated offshore Viana do Castelo, Portugal. The farm's primary objective was to harness wave energy while simultaneously protecting a co-located wind farm from waves, in order to increase the weather windows for operation and maintenance.

The key findings of the study are as follows:

- K-means clustering effectively reduced the number of sea states required for the accurate wave farm simulations while preserving at least 90 % of the incoming wave energy. However, it is crucial to acknowledge that k-means clustering utilizes Euclidean distance, which is not well-suited for analyzing data with circular characteristics, such as wave direction. This limitation was overcome by restricting wave directions to a sector lower than 180°. Alternatively, employing specialized distance metrics for circular data representation could be explored in future works;
- The GA configured with a 70 % crossover rate, a population size of 25 individuals, and an elite rate of 12 % achieved the optimal balance between solution quality and computational efficiency. Importantly, this approach leverages a continuous domain for WEC placement. Unlike traditional grid-based methods that restrict WEC positions to pre-defined locations, the GA allows for a more nuanced and potentially superior optimization by enabling free positioning within the designated area;
- Compared to a previous study with a non-optimized layout design, the proposed GA method yielded a significant improvement in both the absorbed wave power (87 % increase) and wave height reduction (46 % increase) within the designated area of interest;
- The limitations of the study include the inherent trade-offs between the optimization objectives (HRA and *q-factor*) and the challenges posed by area restrictions due to a large number of WECs or wide inter-device spacing.

In essence, this study demonstrates the effectiveness of the GA in optimizing wave farm layouts for efficient wave energy capture while simultaneously mitigating negative wave impacts on co-located wind farms. The proposed methodology, particularly the utilization of a continuous domain and the versatile SNL-SWAN model, is valuable for advancing the development and implementation of wave farms. The vast range of inputs and outputs allowed by SNL-SWAN model enhances the applicability and comparability of this framework across diverse WEC technologies and environmental conditions.

This finding underscores the nuanced interplay between different performance metrics within multi-objective optimization frameworks. It suggests that achieving the most favorable outcome needs a holistic evaluation of various parameters and their respective trade-offs, rather than focusing solely on individual metrics. Such insights are instrumental in refining optimization strategies and enhancing the effectiveness of WEC layout design processes.

Future work entails the incorporation of economic valuation within the WLA, specifically through the integration of LCoE assessments for both wave and wind farms. Additionally, there is a focus on environmental impact evaluation, particularly in the context of WEC farms installed in nearshore environments. These endeavors aim to provide a more comprehensive understanding of the economic viability and environmental sustainability of integrated renewable energy systems.

To foster further R&D in the area, the GA code, as well as the pre- and post-processing codes used, are made available on the GitHub repository https://github.com/FelipeTDuarte/GA_WEC_farm_optimization. This will enable researchers to replicate the findings, explore modifications to the algorithm, and adapt the framework to different conditions. By facilitating collaboration and knowledge sharing, this open-source approach can accelerate the progress towards optimized and efficient wave energy farms.

CRediT authorship contribution statement

Felipe Teixeira-Duarte: Writing – original draft, Visualization, Validation, Software, Methodology, Investigation, Formal analysis, Data curation, Conceptualization. **Paulo Rosa-Santos:** Writing – review & editing, Validation, Supervision, Resources, Project administration, Methodology, Funding acquisition, Conceptualization. **Francisco Taveira-Pinto:** Writing – review & editing, Validation, Supervision, Resources, Project administration, Methodology, Funding acquisition, Conceptualization.

Funding sources

The first author acknowledges the funding in the form of a Ph.D. scholarship grant by the FCT, co-financed by the EU's ESF through the NORTE 2020 program, with reference 2020.09157.BD. Furthermore, during this research study. This work was also funded by the project ATLANTIDA (NORTE-01-0145-FEDER-000040), supported by the North Portugal Regional Operational Programme (NORTE2020), under the PORTUGAL 2020 Partnership Agreement and through the European Regional Development Fund (ERDF).

Declaration of competing interest

The authors declare that they have no known competing financial interests or personal relationships that could have appeared to influence the work reported in this paper.

References

[1] F. Taveira-Pinto, P. Rosa-Santos, T. Fazeres-Ferradosa, Marine renewable energy, Renew. Energy 150 (2020) 1160–1164, https://doi.org/10.1016/j.renene.2019.10.014.
[2] F. Teixeira-Duarte, D. Clemente, G. Giannini, P. Rosa-Santos, F. Taveira-Pinto, Review on layout optimization strategies of offshore parks for wave energy converters, Renew. Sustain. Energy Rev. 163 (2022) 112513, https://doi.org/10.1016/J.RSER.2022.112513.
[3] Grupo de Trabalho para o planeamento e operacionalização de centros electroprodutores baseados em fontes de energias renováveis de origem ou localização oceânica (Despacho n.º 11404/2022 de 23 de setembro). Relatório do Grupo de Trabalho para o planeamento e operacionalização de centros eletroprodutores renováveis de origem ou localização oceânica, 2023.
[4] C.E. Clark, G. Barter, K. Shaler, B. DuPont, Reliability-based layout optimization in offshore wind energy systems, Wind Energy 25 (2022) 125–148, https://doi.org/10.1002/we.2664.
[5] D. McMillan, G.W. Ault, Condition monitoring benefit for onshore wind turbines: sensitivity to operational parameters, IET Renew. Power Gener. 2 (2008) 60–72, https://doi.org/10.1049/IET-RPG:20070064.
[6] C.E. Clark, A. Miller, B. DuPont, An analytical cost model for co-located floating wind-wave energy arrays, Renew. Energy 132 (2019) 885–897, https://doi.org/10.1016/J.RENENE.2018.08.043.
[7] S. Astariz, G. Iglesias, Accessibility for operation and maintenance tasks in co-located wind and wave energy farms with non-uniformly distributed arrays, Energy Convers. Manag. 106 (2015) 1219–1229, https://doi.org/10.1016/j.enconman.2015.10.060.
[8] S. Astariz, G. Iglesias, Enhancing wave energy competitiveness through Co-located wind and wave energy farms. A review on the shadow effect, Energies 8 (2015) 7344–7366, https://doi.org/10.3390/en8077344.
[9] S. Astariz, C. Perez-Collazo, J. Abanades, G. Iglesias, Hybrid wave and offshore wind farms: a comparative case study of co-located layouts, International Journal of Marine Energy 15 (2016) 2–16, https://doi.org/10.1016/j.ijome.2016.04.016.
[10] S. Astariz, J. Abanades, C. Perez-Collazo, G. Iglesias, Improving wind farm accessibility for operation & maintenance through a co-located wave farm: influence of layout and wave climate, Energy Convers. Manag. 95 (2015) 229–241, https://doi.org/10.1016/j.enconman.2015.02.040.
[11] S. Astariz, A. Vazquez, M. Sánchez, R. Carballo, G. Iglesias, Co-located wave-wind farms for improved O&M efficiency, Ocean Coast Manag. 163 (2018) 66–71, https://doi.org/10.1016/j.ocecoaman.2018.04.010.
[12] S. Astariz, C. Perez-Collazo, J. Abanades, G. Iglesias, Co-located wave-wind farms: economic assessment as a function of layout, Renew. Energy 83 (2015) 837–849, https://doi.org/10.1016/j.renene.2015.05.028.
[13] S. Astariz, C. Perez-Collazo, J. Abanades, G. Iglesias, Co-located wind-wave farm synergies (Operation & Maintenance): a case study, Energy Convers. Manag. 91 (2015) 63–75, https://doi.org/10.1016/j.enconman.2014.11.060.
[14] F. Teixeira-Duarte, V. Ramos, P. Rosa-Santos, F. Taveira-Pinto, Multi-objective decision tool for the assessment of co-located wave-wind offshore floating energy

parks, Ocean Eng. 292 (2024) 116449, https://doi.org/10.1016/J.OCEANENG.2023.116449.
[15] L. Cui, N.Y. Sergiienko, J.S. Leontini, N. Cohen, L.G. Bennetts, B. Cazzolato, et al., Protecting coastlines by offshore wave farms: on optimising array configurations using a corrected far-field approximation, Renew. Energy 224 (2024) 120109, https://doi.org/10.1016/j.renene.2024.120109.
[16] Z. Cheng, T.R. Wen, M.C. Ong, K. Wang, Power performance and dynamic responses of a combined floating vertical axis wind turbine and wave energy converter concept, Energy 171 (2019) 190–204, https://doi.org/10.1016/J.ENERGY.2018.12.157.
[17] C. Pérez-Collazo, D. Greaves, G. Iglesias, A review of combined wave and offshore wind energy, Renew. Sustain. Energy Rev. 42 (2015) 141–153, https://doi.org/10.1016/J.RSER.2014.09.032.
[18] C. Perez-Collazo, S. Astariz, J. Abanades, D. Greaves, G. Iglesias, CO-LOCATED wave and offshore wind farms: a preliminary case study of an hybrid array, Coastal Engineering Proceedings 1 (2014) 33, https://doi.org/10.9753/icce.v34.structures.33.
[19] J. Abanades, D. Greaves, G. Iglesias, Coastal defence through wave farms, Coast Eng. 91 (2014) 299–307, https://doi.org/10.1016/j.coastaleng.2014.06.009.
[20] J. Abanades, G. Flor-Blanco, G. Flor, G. Iglesias, Dual wave farms for energy production and coastal protection, Ocean Coast Manag. 160 (2018) 18–29, https://doi.org/10.1016/j.ocecoaman.2018.03.038.
[21] P. Balitsky, N. Quartier, V. Stratigaki, G.V. Fernandez, P. Vasarmidis, P. Troch, Analysing the near-field effects and the power production of near-shore WEC array using a new wave-to-wire model. https://doi.org/10.3390/w11061137, 2019.
[22] R.J. Bergillos, A. López-Ruiz, E. Medina-López, A. Moñino, M. Ortega-Sánchez, The role of wave energy converter farms on coastal protection in eroding deltas, Guadalfeo, southern Spain, J. Clean. Prod. 171 (2018) 356–367, https://doi.org/10.1016/j.jclepro.2017.10.018.
[23] D.L. Millar, H.C.M. Smith, D.E. Reeve, Modelling analysis of the sensitivity of shoreline change to a wave farm, Ocean Eng. 34 (2007) 884–901, https://doi.org/10.1016/J.OCEANENG.2005.12.014.
[24] E. Luczko, B. Robertson, H. Bailey, C. Hiles, B. Buckham, Representing non-linear wave energy converters in coastal wave models, Renew. Energy 118 (2018) 376–385, https://doi.org/10.1016/J.RENENE.2017.11.040.
[25] Project Overview — SNL-SWAN n.d. https://snl-waterpower.github.io/SNL-SWAN/(accessed January 18, 2023).
[26] K. Ruehl, A. Porter, A. Posner, J. Roberts, Development of SNL-SWAN, a validated wave energy converter array modeling tool. Proceedings of the 10th European Wave and Tidal Energy Conference, 2013.
[27] K. Ruehl, A. Porter, C. Chartrand, H. Smith, G. Chang, J. Roberts, Development, verification and application of the SNL-SWAN open source wave farm code. Proceedings of the 11th European Wave and Tidal Energy Conference, Nantes, France, 2015.
[28] A. Porter, K. Ruehl, C. Chartrand, H. Smith, Development and release of the open-source wave climate environment assessment tool snl-swan. Proceedings of the 3rd Marine Energy Technology Symposium, Washington, DC, USA, 2015.
[29] B. Yang, S. Wu, H. Zhang, B. Liu, H. Shu, J. Shan, et al., Wave energy converter array layout optimization: a critical and comprehensive overview, Renew. Sustain. Energy Rev. 167 (2022) 112668, https://doi.org/10.1016/J.RSER.2022.112668.
[30] M. Folley, A. Babarit, B. Child, D. Forehand, L. O'boyle, K. Silverthorne, et al., A review of numerical modelling of wave energy converter arrays A review of numerical modelling of wave energy converter arrays A REVIEW OF NUMERICAL MODELLING OF WAVE ENERGY CONVERTER ARRAYS. https://doi.org/10.1115/OMAE2012, 2012.
[31] L. Cuadra, S. Salcedo-Sanz, J.C. Nieto-Borge, E. Alexandre, G. Rodríguez, Computational intelligence in wave energy: comprehensive review and case study, Renew. Sustain. Energy Rev. 58 (2016) 1223–1246, https://doi.org/10.1016/j.rser.2015.12.253.
[32] M. Göteman, M. Giassi, J. Engström, J. Isberg, Advances and challenges in wave energy park optimization—a review, Front. Energy Res. 8 (2020), https://doi.org/10.3389/fenrg.2020.00026.
[33] B.F.M. Child, V. Venugopal, Optimal configurations of wave energy device arrays, Ocean Eng. 37 (2010) 1402–1417, https://doi.org/10.1016/j.oceaneng.2010.06.010.
[34] M. Giassi, M. Göteman, Layout design of wave energy parks by a genetic algorithm, Ocean Eng. 154 (2018) 252–261, https://doi.org/10.1016/j.oceaneng.2018.01.096.
[35] M. Göteman, J. Engström, M. Eriksson, J. Isberg, Fast modeling of large wave energy farms using interaction distance cut-off, Energies 8 (2015) 13741–13757, https://doi.org/10.3390/en81212394.
[36] M. Giassi, M. Göteman, S. Thomas, J. Engström, M. Eriksson, J. Isberg, Multi-parameter optimization of hybrid arrays of point absorber wave energy converters. 12th European Wave and Tidal Energy Conference (EWTEC), Cork, Ireland, 2017. August 27-31, 2017.
[37] S. Bozzi, M. Giassi, A. Moreno Miquel, A. Antonini, F. Bizzozero, G. Gruosso, et al., Wave energy farm design in real wave climates: the Italian offshore, Energy 122 (2017) 378–389, https://doi.org/10.1016/j.energy.2017.01.094.
[38] D. Sarkar, E. Contal, N. Vayatis, F. Dias, Prediction and optimization of wave energy converter arrays using a machine learning approach, Renew. Energy 97 (2016) 504–517, https://doi.org/10.1016/j.renene.2016.05.083.
[39] H.A. Wolgamot, P.H. Taylor, R. Eatock Taylor, The interaction factor and directionality in wave energy arrays, Ocean Eng. 47 (2012) 65–73, https://doi.org/10.1016/j.oceaneng.2012.03.017.
[40] M. Vicente, M. Alves, A. Sarmento, Layout optimization of wave energy point absorbers arrays. 10th European Wave and Tidal Energy Conference Series, Aalborg, Denmark, 2013.
[41] M.M. Moarefdoost, L.V. Snyder, B. Alnajjab, Layouts for ocean wave energy farms: models, properties, and optimization, Omega (Westport) 66 (2017) 185–194, https://doi.org/10.1016/j.omega.2016.06.004.
[42] L.V. Snyder, M.M. Moarefdoost, LAYOUTS FOR OCEAN WAVE ENERGY FARMS: MODELS, PROPERTIES, AND HEURISTIC, Marine Energy Technology Symposium, 2014.
[43] M. Neshat, B. Alexander, M. Wagner, A hybrid cooperative co-evolution algorithm framework for optimising power take off and placements of wave energy converters, Inf. Sci. 534 (2020) 218–244, https://doi.org/10.1016/j.ins.2020.03.112.
[44] M. Neshat, S. Mirjalili, N.Y. Sergiienko, S. Esmaeilzadeh, E. Amini, A. Heydari, et al., Layout optimisation of offshore wave energy converters using a novel multi-swarm cooperative algorithm with backtracking strategy: a case study from coasts of Australia, Energy 239 (2022) 122463, https://doi.org/10.1016/J.ENERGY.2021.122463.
[45] S. Astariz, C. Perez-Collazo, J. Abanades, G. Iglesias, Towards the optimal design of a co-located wind-wave farm, Energy 84 (2015) 15–24, https://doi.org/10.1016/j.energy.2015.01.114.
[46] J. Izquierdo-Pérez, B.M. Brentan, J. Izquierdo, N.-E. Clausen, A. Pegalajar-Jurado, N. Ebsen, Layout optimization process to minimize the cost of energy of an offshore floating hybrid wind–wave farm, Processes 8 (2020) 139, https://doi.org/10.3390/pr8020139.
[47] D. Golbaz, R. Asadi, E. Amini, H. Mehdipour, M. Nasiri, B. Etaati, et al., Layout and design optimization of ocean wave energy converters: a scoping review of state-of-the-art canonical, hybrid, cooperative, and combinatorial optimization methods, Energy Rep. 8 (2022) 15446–15479, https://doi.org/10.1016/J.EGYR.2022.10.403.
[48] J.D. Roberts, G. Chang, J. Magalen, C. Jones, Wave energy converter effects on wave fields: evaluation of SNL-SWAN and sensitivity studies in monterey bay CA. https://doi.org/10.2172/1156934, 2014.
[49] Projeto WindFLoat Atlantic | edp.com n.d. https://www.edp.com/pt-pt/inovacao/windfloat (accessed November 14, 2022).
[50] Direção-Geral de Recusos Naturais S e SM (DGRM), TUPEM Nº 1/2015, 2015.
[51] Instituto hidrográfico, Avisos Aos Navegantes, 2022 aviso 245/22.
[52] P. Rosa-Santos, F. Taveira-Pinto, C.A. Rodríguez, V. Ramos, M. López, The CECO wave energy converter: recent developments, Renew. Energy 139 (2019) 368–384, https://doi.org/10.1016/J.RENENE.2019.02.081.
[53] P. Rosa-Santos, F. Taveira-Pinto, L. Teixeira, J. Ribeiro, CECO wave energy converter: experimental proof of concept, J. Renew. Sustain. Energy 7 (2015) 061704, https://doi.org/10.1063/1.4938179.
[54] G. Giannini, P. Rosa-Santos, V. Ramos, F. Taveira-Pinto, On the development of an offshore version of the CECO wave energy converter, Energies 13 (2020) 1036, https://doi.org/10.3390/EN13051036, 2020;13:1036.
[55] M. López, F. Taveira-Pinto, P. Rosa-Santos, Numerical modelling of the CECO wave energy converter, Renew. Energy 113 (2017) 202–210, https://doi.org/10.1016/J.RENENE.2017.05.066.
[56] P. Rosa-Santos, F. Taveira-Pinto, J. Pinho-Ribeiro, L. Teixeira, J. Marinheiro, Harnessing the kinetic and potential wave energy: design and development of a new wave energy converter, Renewable Energies Offshore (2015) 367–374.
[57] V. Ramos, G. Giannini, T. Calheiros-Cabral, M. López, P. Rosa-Santos, F. Taveira-Pinto, Assessing the effectiveness of a novel WEC concept as a Co-located solution for offshore wind farms, J. Mar. Sci. Eng. 10 (2022) 267, https://doi.org/10.3390/JMSE10020267, 2022;10:267.
[58] SNL-SWAN/bin at master · SNL-WaterPower/SNL-SWAN · GitHub n.d. https://github.com/SNL-WaterPower/SNL-SWAN/tree/master/bin (accessed January 18, 2023).
[59] V. Ramos, M. López, F. Taveira-Pinto, P. Rosa-Santos, Influence of the wave climate seasonality on the performance of a wave energy converter: a case study, Energy 135 (2017) 303–316, https://doi.org/10.1016/J.ENERGY.2017.06.080.
[60] P. Camus, F.J. Mendez, R. Medina, A.S. Cofiño, Analysis of clustering and selection algorithms for the study of multivariate wave climate, Coast Eng. 58 (2011) 453–462, https://doi.org/10.1016/J.COASTALENG.2011.02.003.
[61] C.A. Hegermiller, J.A.A. Antolinez, A. Rueda, P. Camus, J. Perez, L.H. Erikson, et al., A multimodal wave spectrum–based approach for statistical downscaling of local wave climate, J. Phys. Oceanogr. 47 (2017) 375–386, https://doi.org/10.1175/JPO-D-16-0191.1.
[62] S. Draycott, T. Davey, D. Ingram, J. Lawrence, A. Day, L. Johanning, Applying Site Specific Resource Assessment: Methodologies for Replicating Real Seas in the FLOWAVE Facility, 2014.
[63] S.T. Draycott, On the re-creation of site-specific directional wave conditions. https://doi.org/10.1016/J.COASTALENG, 2017.
[64] L.J. Hamilton, Characterising spectral sea wave conditions with statistical clustering of actual spectra, Appl. Ocean Res. 32 (2010) 332–342, https://doi.org/10.1016/J.APOR.2009.12.003.
[65] D. Wang, S. Jin, M. Hann, D. Conley, K. Collins, D. Greaves, Power output estimation of a two-body hinged raft wave energy converter using HF radar measured representative sea states at Wave Hub in the UK, Renew. Energy 202 (2023) 103–115, https://doi.org/10.1016/J.RENENE.2022.11.048.
[66] W.K. Eymold, C. Flanary, L. Erikson, K. Nederhoff, C.C. Chartrand, C. Jones, et al., Typological representation of the offshore oceanographic environment along the Alaskan North Slope, Continent. Shelf Res. 244 (2022) 104795, https://doi.org/10.1016/J.CSR.2022.104795.

[67] E. Romano-Moreno, G. Diaz-Hernandez, A. Tomás, J.L. Lara, Multivariate assessment of port operability and downtime based on the wave-induced response of moored ships at berths, Ocean Eng. 283 (2023) 115053, https://doi.org/10.1016/J.OCEANENG.2023.115053.
[68] E. Romano-Moreno, G. Diaz-Hernandez, A. Tomás, J.L. Lara, Multimodal harbor wave climate characterization based on wave agitation spectral types, Coast Eng. 180 (2023) 104271, https://doi.org/10.1016/J.COASTALENG.2022.104271.
[69] F. Pedregosa Fabianpedregosa, V. Michel, O. Grisel Oliviergrisel, M. Blondel, P. Prettenhofer, R. Weiss, et al., Scikit-learn: machine learning in Python, J. Mach. Learn. Res. 12 (2011) 2825–2830.
[70] D. Clemente, F. Teixeira-Duarte, P. Rosa-Santos, F. Taveira-Pinto, Advancements on optimization algorithms applied to wave energy assessment: an overview on wave climate and energy resource, Energies 16 (2023) 4660, https://doi.org/10.3390/EN16124660, 2023;16:4660.
[71] A.E. Eiben, J.E. Smith, Introduction to Evolutionary Computing, second ed., Springer Berlin Heidelberg, Berlin, Heidelberg, 2015 https://doi.org/10.1007/978-3-662-44874-8.
[72] A.G. Conzalez-Rodriguez, J. Serrano-Conzalez, J.M. Riquelme-Santos, M. Burgos-Payán, J. Castro-Mora, S.A. Persan, Global optimization of wind farms using evolutive algorithms, Wind Power Systems (2010) 53–104, https://doi.org/10.1007/978-3-642-13250-6_3.
[73] M. Kubat, An Introduction to Machine Learning, second ed., Springer International Publishing, 2015 https://doi.org/10.1007/978-3-319-20010-1.